

Revisiting Electrocatalytic CO₂ Reduction in Nonaqueous Media: Promoting CO₂ Recycling in Organic Molecules by Controlling H₂ Evolution

Eduardo Arizono dos Reis, Gelson T. S. T. da Silva, Elisabete I. Santiago, and Caue Ribeiro*

Electrochemical CO₂ reduction to fuels or commodity chemicals using renewable energy has drawn attention as a strategy for closing the anthropogenic chemical carbon cycle. More than that, enhancing the C–C coupling between the intermediates could lead to producing a range of high-value multi-carbon molecules. Although the research mainly focuses on the aqueous media for the electrochemical CO₂ reduction reaction (eRRCO₂), using nonaqueous electrolytes has the advantage of suppressing the hydrogen evolution reaction, controlling the proton-assisted reduction reactions, and favoring the C–C coupling. Herein, the use of nonaqueous electrolytes for eRRCO₂ and the components of the electrochemical reactor that affect the selectivity of the reaction are revisited. This review provides a perspective view of recent findings compared to well-established papers while presenting what is known about eRRCO₂ in nonaqueous media.

1. Introduction

With the industrial revolution and the merging of technology and industry, technical innovation has brought technologies that impact people's daily lives.^[1] As a result of technological evolution, higher levels of environmental pollution have become a cause of great concern nowadays.^[2] One of the biggest worries is the emission and accumulation of greenhouse gases (GHG) due to their impact on the environment and human life. The leading gases classified as GHG are carbon dioxide (CO₂), methane (CH₄), nitrous oxide (N₂O), and fluorinated. Among them, CO₂ corresponded to 79% of the emissions in 2020,^[3] and many

technologies have been developed to capture and SEQUESTrate the CO₂ and mitigate its anthropogenic emission to the atmosphere.^[2,4] This way, instead of a waste end-product, CO₂ can be used as a cheap and abundant feedstock to obtain carbon-neutral value-added chemicals.^[1,4]

In recent years, electrochemical reduction of carbon dioxide has been gaining attention as an efficient method to convert CO₂ into value-added products.^[5] The electrochemical CO₂ reduction reaction (eCO₂RR) can be coupled with renewable energy and stands out over the other conversion methods because it operates under mild conditions of temperature and pressure, allows the control of the reaction by adjusting external parameters, can be


tuned to selective products, and could be integrated to CO₂ sources in the industry, like fermentation plant and carbon-intensive manufacturing industries.^[4–6] Despite advances in electrocatalytic CO₂ reduction, the unsatisfactory selectivity, costly separation steps, and the deactivation of electrodes (typically less than 100 h) restrict practical use and technological commercialization. The growing and necessary advances related to the role of the catalyst in the conversion of CO₂ into products demonstrate only one side of the search for more selective and efficient processes, while phenomena behind the architecture of the electrodes and catalytic reactors exhibit another effective way to increase the electrocatalytic performance of the system under mild operational conditions.^[7] In this sense, from an industrial point of view, replacing water with organic solvents can modulate the selectivity and facilitate the separation of CO₂ reduction products—unlike water, which forms an azeotropic solution with some molecules obtained from eCO₂RR.

The use of nonaqueous electrolytes is interesting since multi-carbon (C₂₊) products can be easily obtained and re-incorporated into the industrial plant or used as a CO₂-neutral molecule to synthesize multicarbon compounds.^[8] Although the advantages of the organic electrolyte, most of the studies focus on the aqueous system, and just a small number of research up to date have investigated the reduction in organic medium.^[9] Additionally, there is a great number of eCO₂RR reviews,^[5,10–13] but a few address it in organic medium.^[14–16] To date, the more comprehensive reference on this topic was a book chapter by Hori, published in 2008.^[17] Here, extensive literature is revised.

E. A. dos Reis, C. Ribeiro
São Carlos Institute of Chemistry
University of São Paulo – USP
São Carlos, São Paulo 13566-590, Brazil
E-mail: caue.ribeiro@embrapa.br

E. A. dos Reis, C. Ribeiro
Nanotechnology National Laboratory for Agriculture (LNNA)
Embrapa Instrumentation
São Carlos, São Paulo 13561-206, Brazil

G. T. S. T. da Silva, E. I. Santiago
Center of Fuel Cells and Hydrogen (CCCH)
Nuclear and Energy Research Institute (IPEN)
São Carlos, São Paulo-SP 13560-970, Brazil

 The ORCID identification number(s) for the author(s) of this article can be found under <https://doi.org/10.1002/ente.202201367>.

DOI: 10.1002/ente.202201367

We provide an in-depth analysis of the publications on electrochemical CO₂ reduction in organic medium, discussing the electrocatalyst efficiency and selectivity factors and the influence of the system configuration on the main product obtained from eCO₂RR. Furthermore, we aim to highlight the improvements that have been made to shorten the gap between laboratory and industry applications.

2. Electrochemical CO₂ Reduction in Organic Media versus Aqueous Medium

Electrochemical CO₂ reduction is challenging due to its linear *sp* hybridized structure, granting high thermodynamic stability to the CO₂ molecule^[18,19] and its low solubility.^[19] In the aqueous system, the carbon dioxide solubility is 34 mmol L⁻¹ (300 K, neutral pH) and may vary slightly depending on the temperature, pressure, concentration, and type of anions in the electrolyte.^[20,21] In this sense, the main advantage of using a nonaqueous electrolyte is the higher solubility of CO₂ and the possibility of complete suppression of hydrogen evolution reaction (HER). The solubilities in water and the principal solvents used in the eCO₂RR are shown in **Figure 1**, noticing that for some nonaqueous solvents, CO₂ solubility is eight times higher than in water. Higher solubility reduces limitations associated with mass transport and achieving industrial-relevant current densities (>100 mA cm⁻²) generated by the low diffusion of CO₂ in aqueous systems.^[22]

Another advantage of choosing an organic solvent is the easiness of controlling the protic viability in the eCO₂RR. It could be the way to overcome the drawback of the wide range of chemical species obtained as a product in aqueous media^[22,23] due to the several proton-assisted multiple-electron-transfer processes with similar standard potentials.^[24,25] Review articles published by Zhang et al.^[26] Ahmad et al.,^[27] Li et al.^[28] can be useful for a better understanding of the reaction in aqueous media.

Furthermore, using nonaqueous electrolytes avoids HER competition with CO₂ reduction, another barrier to achieving

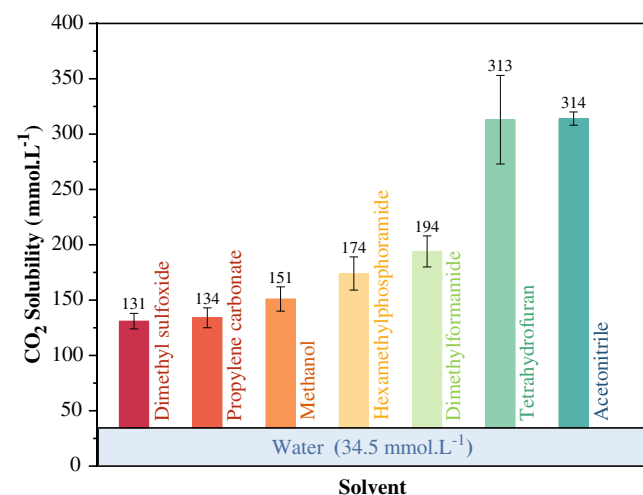


Figure 1. CO₂ solubilities of principal solvents used in the eCO₂RR at *p* = 101.3 kPa and *T* = 25 °C. Mean solubilities data extracted from ref. [15].

industrial-relevant selectivity and efficiency.^[23] Also, considering that the coupling of the CO₂ intermediates to forming C₂₊ products requires the diffusion and adsorption of several CO₂ molecules to the catalyst surface, stepwise transformation, and spatial positioning,^[22] the organic electrolyte can enable efficient production of more available multicarbon chemicals by stabilizing the intermediates and avoiding proton-assisted multiple-electron-transfer processes. Although ionic liquids present similar advantages when compared to the use of an aqueous solution, they were not considered since it has the maturity to be addressed in an exclusive review as done by Lim and Kim;^[29] Feng and co-authors;^[30] Faggion et al.,^[31] Yang and co-authors;^[32] Mohammed et al.^[33]

3. Experimental Devices for Nonaqueous eCO₂RR

Teeter and Rysseberghe first realized the electrochemical conversion of CO₂ in 1954.^[34] At that time, the authors sought to prove from electrolysis curves that the cathodic process observed in polarization experiments was related to the reduction of CO₂ into formic acid and not to hydrogen evolution. The first CO₂ conversion experiments were performed in a concept inherited by hydrogen evolution (HER), a single-chamber design. In a typical electrolytic cell, the working, reference, and counter electrodes are located close to each other in the same chamber, reducing the ohmic resistance between electrodes.^[35] However, in reactions conducted in aqueous media, the oxygen molecules generated at the anode (by water oxidation) are moved to the cathode electrode. They can be reduced, producing unwanted hydrogen and oxidizing species that can oxidize the produced carbonaceous chemicals, thus substantially decreasing the energy conversion efficiency.^[24]

In contrast, CO₂ conversion in nonaqueous media using an undivided cell achieves effective CO₂ reduction efficiency but leads mostly to aprotic products such as carbon monoxide (CO) or oxalate (C₂O₄²⁻). Rudnev and co-workers^[36] demonstrate an increase in cathodic current density attributed to converting CO₂ to CO in acetonitrile and polypropylene using copper-modified platinum crystals as the catalyst. The authors report that using an aprotic electrolyte is intended to increase current density and avoid parallel reactions that could block the electrode surface, making it difficult to interpret the results of interest, the investigation of the structural effect of Cu-modified electrodes.

Furthermore, this cell design allows the formation of products from the consumption of sacrificial agents,^[37] either dissolved in solution^[37,38] or generated by ion release at the anode.^[39,40] The electrolysis of CO₂ in dry acetonitrile, absent of water, can be performed at a higher application potential promoting dimerization of CO₂ molecules at the metals (lead and steel 304) electrode (cathode). At the same time, zinc ions (Zn²⁺) were released at the anode, successfully promoting the synthesis of Zn₂C₂O₄ by electrochemical pathway and avoiding its consecutive reduction. Although simple and pioneering, this cell configuration was quickly exchanged for the H-type electrochemical cell (H-Cell) design. This conformation allows CO₂ reduction reactions on a lab scale in a simple and efficient path because its main feature is the presence of an ion-exchange membrane

separating the cathodic reactions (CO₂RR) from the anodic reactions (OER), producing independent reactions. Therefore, in this configuration, the cathode chamber is composed of a working electrode and a reference electrode, while on the anodic side, the counter electrode is positioned.

Kaiser and Heiz^[41] pioneering developed that configuration in 1973, conducting electrochemical reactions using materials (Pb, Hg, Pt, and C) and aprotic electrolytes (acetonitrile (AN), propylene carbonate (PC), hexamethylphosphoramide (HMPA), and membranes (cationic or anionic). From these results, the authors describe that the reaction path will depend on the strength with which the molecule will be chemically adsorbed on the surface of the material—intensely chemisorbed materials are driven to carbonate (CO₃²⁻), and weakly nucleophilic electrolytes such as propylene carbonate, acetonitrile will drive oxalate (C₂O₄²⁻) formation. Furthermore, the configuration used allows the protons from the anodic chamber (H₂SO₄) to migrate to the cathodic side, favoring the formation of oxalic acid (H₂C₂O₄) instead of formic acid (HCOOH) under specific conditions. Using a sacrificial electrode as the anode for the selectivity formation of zinc oxalate is also possible.^[9] While this cell design allows the control of selectivity by changing the ions in the anolyte (and the membrane), its main disadvantage is the high interelectrode distance, which implies the need for high overpotentials and low energy efficiency.

Recent studies have featured conducting CO₂ reduction experiments using near-zero gap flow cells to increase CO₂ conversion and decrease the presence of protons at the cathode. One successful example is the work by V. Boor and co-workers,^[42] where they describe the use of GDL electrodes in filter press reactors to evaluate the electrocatalytic efficiency of Pb nanoparticles under flow cells. The GDL electrode architecture has allowed for larger electrically active areas, while percolation of the gas into propylene carbonate further increases the local CO₂ concentration. The authors report faradaic efficiencies to achieve around 60% at −2.5 V versus Ag/AgCl, with current densities ≈10 mA cm^{−2}, 2.5 times higher than H-cell (4 mA cm^{−2}) after 1 h. In parallel, König and co-workers^[9] used the same cell configuration to achieve faradaic efficiency above 53%, with a current density over 40 times higher (80 mA cm^{−2}), using a pure lead electrode, demonstrating that the evolution of experimental setups for the conversion of CO₂ into products in nonaqueous media is constantly evolving and that it is expected that soon it may be possible to apply this promising pathway for chemical energy storage on a large scale.

4. Ion Exchange Membranes

In conventional electrochemistry, the electrolytes (ion carriers) of choice are aqueous solutions due to their simplicity of preparation and handling, the wide variety of carrier ions with different ionic mobility, and the cost. However, disadvantages such as narrow potential window, limited by H₂ and O₂ evolution reactions (REH and REO), the low solubility of gases (such as CH₄, CO₂, etc.), and constant need for concentration and ionic strength correction in continuous operation systems, make the use of aqueous electrolytes quite restricted, especially in electrochemical reactors.

Most CO₂ reduction reactions are conducted using ion exchange membranes, either in H-type or flow-through reactors, because this part of the device limits the reoxidation of the product, aiding in the efficiency of the reaction while keeping the electrical circuit closed, allowing the passage of the ions generated in the cathode and anode chambers. In addition, membrane reactors, in which the ion exchange membrane acts as a solid electrolyte and physical barrier, have also been considered a key component for solid-state-based CO₂ reduction devices.^[43]

Solid electrolytes based on ion exchange membranes (IEM) constitute a relevant class of dense polymeric membranes (solid) with functional groups with ionic species bound to the polymer matrix, also called ionomeric membranes. These membranes allow ions of opposite charge (counterions) to be selectively conducted between the functional groups, thus generating the ionic conduction mechanism. This electrolyte has become a critical component in water desalination processes and electrolysis. At present, it is very firmly in energy storage and conversion systems, such as fuel cells.^[44] Specifically for IEMs, ionic conductivity, ionic strength, and pH are directly related to the counterion, and, in this context, IEMs are divided into 1) cation exchange membranes (CEM); and 2) anion exchange membranes (AEM).

The electrolyte must have the following characteristics for the cell to have a high efficiency considering the application in gas-phase electrochemical membrane reactors:^[45] 1) High ion conductivity and minimal resistive loss; 2) It must be insulating (no electronic conductivity), otherwise the electron will not go through the external circuit but through the membrane, reducing the useful power; 3) Adequate chemical and mechanical stability to allow assembly and operation in electrochemical devices; 4) Low fuel permeability, minimizing crossing through the membrane (crossover); and 5) Production costs adequate to the application, aiming to make the technology economically viable for real applications.

Anion-exchange membranes (AEMs) have gained significant attention in the past 10 years due to their extensive applicability in electrochemical devices, such as fuel cells^[46] and electrolyzers,^[47] replacing proton-exchange membranes (PEMs). The main advantages of AEMs over PEMs in fuel cells are the significantly lower cost compared to state-of-the-art acid membrane (Nafion), less corrosive environment, and substantially lower crossover of fuels from the anode to the cathode.

However, despite the impressive performance advancement, the use of AEMs is still limited by their chemical, thermal, and mechanical stabilities, along with their intrinsic ionic conductivity.^[48] Overall, the AEMs stability strongly depends on the functional groups capable of conducting hydroxide anions^[49] and the polymer backbone.^[50] During operation, the high alkalinity of the medium (hydroxide attacks) is ascribed to be the principal cause of AEMs degradation.^[51]

Even in organic medium, the most used cation exchange membrane is Nafion, a conductive polymer selective to allow the migration of cations (protons) from one chamber to another, offering high chemical and mechanical stabilities. Nafion is a perfluorinated copolymer composed of a polytetrafluorocarbon (PTFE) chain and vinyl ether side chains with sulfonic terminations (SO₃H). This material has excellent chemical and mechanical stability due to its PTFE and structure and excellent proton conductivity due to the hydrophilic sulfonic group.

Under hydrated conditions, the transport of protons and hydroxide at the molecular level is described through two mechanisms: the hydrogen-bond hopping of protons, also called the Grotthuss Mechanism, and/or Vehicular Mechanism, in which water (i.e., bonded water in membrane structure) behaves as a vehicle for ion transport. In the vehicular mechanism, the hydronium ion (hydrated proton) diffuses through the aqueous medium in response to the electrochemical potential difference.^[52] It is a limitation for Nafion utilization in the organic medium since contamination with water cannot, in principle, be avoided. The transport rate depends on the existence of free volumes within the polymeric chains, just as on the vehicular diffusion rate.^[53] Furthermore, water plays an essential role in proton conductivity by impacting the formation, size, connectivity, and strength of ionic pathways and clusters in membranes.^[54] When the cluster size increases under aqueous conditions, the proton conductivity rises along with the degree of hydration.^[55]

More recently, AEMs have been considered an anion-conductive alternative for electrochemical membrane reactors operating in alkaline medium. The development of AEMs is recent and incipient, but it has been rapidly growing due to numerous applications, such as alkaline electrolysis, desalination, and CO₂ conversion.^[56–58] AEM and PEM strongly depend on water to promote ionic conduction due to ion transport mechanisms, such as Grotthuss and vehicular, which intrinsically involve water molecules.

For a very water-sensitivity system, for example, CO₂ conversion in C₂₊ compounds, in which the dimerization of CO₂ molecules occurs exclusively in the absence of water at low pHs, the development of nonaqueous solid electrolytes is crucial for the application of solid electrolytes in electrochemical devices. In this context, polybenzimidazole (PBI)-based membranes become an exciting alternative over the state-of-the-art Nafion-based electrolytes. PBI or poly[2,2-(*m*-phenylene)-5,5-dibenzimidazole belongs to the family of nonperfluorinated membranes and is a polymer known for having high mechanical, thermal and chemical resistance. Despite its recognized mechanical properties, PBI does not present, as found, the capacity to transport ions, an exclusive characteristic of ionomeric polymers. Thus, applying PBI as a solid electrolyte is only possible through doping with inorganic acids, which present some degree of ionic dissociation for application in nonaqueous electrochemical reactors.^[59]

The doping occurs by immersing the pure PBI membrane in a phosphoric acid solution. When submerged, the absorption of the acid solution begins, usually reaching an equilibrium point that can change according to the conditions of the doping solution, such as temperature, concentration, and immersion time. However, changes in dimensions, such as thickness and area of the membrane, are observed in the doping process. Previous studies have shown that the PBI chains can be arranged in a parallel position (stack module form) to the membrane surface and that the doping process can increase the spacing between the chains.^[60] Thus, although volume changes occur proportionally to the degree of doping, a higher variation in thickness is observed than in area.^[61] Such a feature is directly related to the loss of mechanical properties of the material. Regarding applicability, PBI has been employed as a nonaqueous electrolyte for CO₂ electroreduction in a membrane reactor, producing

added-value compounds, such as methanol and acetaldehyde.^[62] However, the literature in the area is promising but scarce.

This membrane and many parts used in CO₂ conversion have its precursor in electrolysis applications. This membrane was used because it allowed the migration of the protons generated in the anodic chamber to the cathodic side, generating hydrogen. However, in CO₂ conversion reactions, where hydrogen evolution is undesirable, although this membrane has been essential, it is losing space to other models, such as anionic membranes.

5. Products and Mechanism of eCO₂RR in Organic Media

The facility control of proton viability, using a nonaqueous solvent, provides more selective eCO₂RR than water. This selectivity is because the reduction of CO₂ in a nonaqueous media starts with the formation of the carbon dioxide radical anion (CO₂^{•-}), and the proton-assisted multiple-electron-transfer processes are avoided. The stabilization of this intermediate can lead to its dimerization and C-C coupling to the formation of C₂₊ products, or it can quickly react with proton donors leading to the formation of C₁ products. Nevertheless, high energy is required to generate the free CO₂^{•-} intermediates from one-electron CO₂ reduction since it occurs at –1.9 V versus NHE or –2.21 V vs. SCE in aprotic solvents (Equation (1)),^[9,63,64] but even higher potentials are usually reported for the eCO₂RR^[63]



At first, it was believed that the formation of the CO₂^{•-} intermediate was directly associated with tetraalkylammonium salts used as supporting electrolytes and that the catalytic effect of NR₄⁺ ions declined as the chain length increased.^[65] More recent publications^[66,67] disposed of the “catalytic” role of NR₄⁺ salts in CO₂ electroreduction in a nonaqueous medium. The diffusion-controlled electroreduction best fits a simple direct outer sphere reduction of dissolved CO₂. The chain length did not exhibit significant changes in the onset potential for eCO₂RR, although the higher current density is observed for longer chain length.^[66]

Due to its extremely short lifetime and high reactivity in either aqueous or nonaqueous solutions,^[68,69] the predominant reaction after the initial formation of CO₂^{•-} depends on factors such as type and pH of the electrolyte, the electrode potential, stirring, the CO₂ partial pressure, and the electrode material.^[70] The intermediate can follow 3 pathways, leading to different products (Figure 2).^[71–74] The only way to form a C₂ product is by dimerizing the dimerization of the CO₂^{•-} (pathway I), leading to oxalic acid formation. Pathways II and III result in C₁ products. Since the proton concentration in the electrolyte can control formic acid formation (pathway II), the primary competitive reaction is through a nucleophilic coupling of radical anion CO₂^{•-} with CO_{2(ads)}, leading to CO and H₂CO₃ (pathway II).^[75]

The proton performs an essential role in the products obtained from eCO₂RR in nonaqueous media, as seen in Figure 2. The control of the electrolyte pH (proton viability) changes the products from their anionic form, and formic acid is produced in low concentrations due to residual water or not being formed. The use of a protic solvent is also expected to serve as a hydrogen

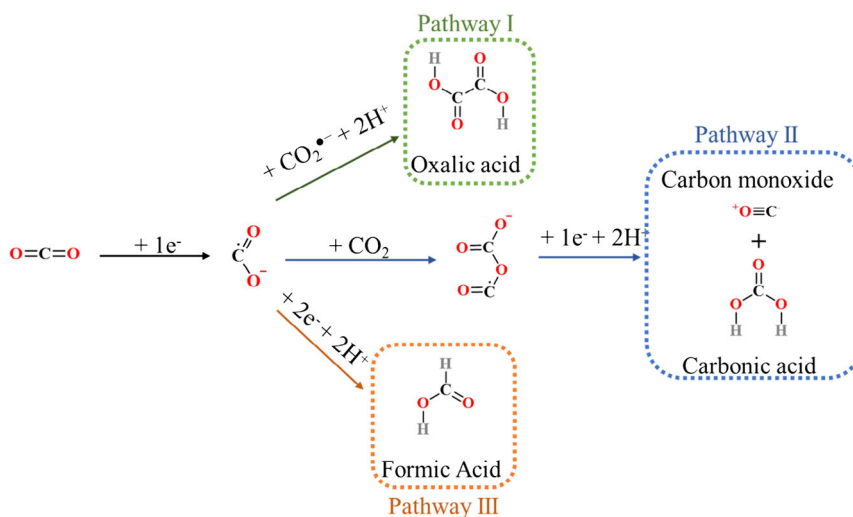


Figure 2. Reaction pathways of eCO₂RR in nonaqueous media.

source for the formation of H₂ and/or hydrocarbons in the system, as demonstrated by Saeki et al.^[76] Still, its anodic degradation was observed, with high efficiency to HER at lower pressure and relatively low concentration of methane and ethylene. The mechanism that leads to the formation of this hydrocarbon resembles the mechanism in water.^[76]

The use of proton donor solvents not only favors the formation of formic acid but also induces further reduction of oxalic acid.^[74] Glyoxylic acid is the first reduction product of oxalic acid (Figure 3), and it is occasionally reported for oxalic acid active catalysts.^[72,74] Eggin et al. observed that longer reaction time and higher potential favor the production of glyoxylic acid and switch the main product. With the increase in glyoxylic acid, the concentration of oxalic acid becomes very low or negligible, and more reduced products are observed. Using methanol as the solvent (a weak proton donor), buffered by the hydroxylamine, and changing the electrolysis potential, it was possible to switch the selectivity of eCO₂RR from oxalic acid to glyoxylic acid and glycolic acid with greatly improved yields.

Although tartaric acid was reported only with trace concentration using nonaqueous media, it is relevant to mention the formation mechanism since it has the potential to be a sustainable selective pathway to obtain C₄ products from CO₂.^[72,77,78] Glyoxylate reduction can occur via two different pathways (Figure 3) that depend on the local pH. With a more alkaline local

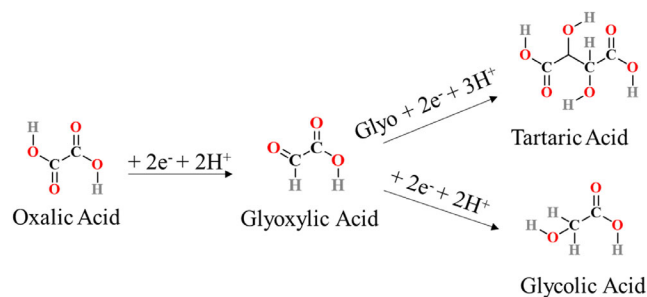


Figure 3. Possible products from oxalic acid reduction.

pH, the formation of tartrate is favored by a one-electron reduction of glyoxylate, followed by its dimerization.

Even though the eCO₂RR using an organic electrolyte is more selective than an aqueous electrolyte, a mixture of different carboxylic acids is usually obtained. Several recovery and purification technologies can be found to purify these products, such as nanofiltration,^[79,80] reverse osmosis,^[80] distillation,^[81,82] and liquid–liquid extraction.^[42,83,84] While the purification technologies are usually studied for aqueous solutions, they can also be applied in nonaqueous solutions, making minor changes and/or combining two or more processes.^[85] The mixture can be avoided using a sacrificial anode (discussed in Section 3), and only liquid–liquid extraction is necessary to purify the CO₂ reduction product.

6. Active Electrocatalysts in Organic Medium

Few electrocatalysts have been reported in the literature for CO₂ reduction in a nonaqueous medium. The literature primarily focuses on homogeneous electrocatalysts; only metal catalysts were thoroughly studied as heterogeneous electrocatalysts in organic electrolytes. This section addresses only heterogeneous catalysts in the literature since homogeneous catalysts are usually synthesized by complex methods with low productivity, inhibiting large-scale applications.^[63] Surveys of homogeneous catalysts for eCO₂RR in organic media have been recently published by Francke et al.,^[86] Franco et al.,^[87] and Kinzel et al.^[88]

Although other authors found out the efficiency of different metals, Pt,^[41] Pb,^[7,74] and Hg^[74] (see Table 1), to electrochemically reduce CO₂ in an organic media, Ikeda et al.^[89] were the first to classify a wide variety of pure metals catalysts by the obtained products. Metal catalysts capable of reducing CO₂ to substantial amounts of oxalic acid and CO were Fe, Cr, Mo, Ni, and Ti and metals that provide only carbon monoxide were Ni, Pd, Pt, and Cu. Ag, Au, Cd, and Sn. Metallic catalysts that selectivity reduce CO₂ to C₂ product were Pb, Tl, and Hg, and only In and Zn were considered inactive due to the small production of oxalic acid.

Table 1. Pure metal catalysts, products, and cell configuration for eCO₂RR in nonaqueous electrolyte.

Electrode	Catholyte ^{a)}	Anolyte	Major products	Cathode potential or j applied	Type of cell	FE [%]	Stability [min.]	References
Pt	PC (H ₂ O traces)		CO and CO ₃ ²⁻	5 mA cm ²	Three compartments	–	–	[41]
Pb	0.3 M Et ₄ NClO ₄ /PC	0.1 M H ₂ SO ₄ /H ₂ O	H ₂ C ₂ O ₄	2.7 V versus Ag/Ag ⁺	Two compartments, aprotic/protic	10	–	[7]
	0.3 M Bu ₄ NBr/Ac	See catholyte	H ₂ C ₂ O ₄	2.0–3.0 V versus Ag/Ag ⁺	Two compartments, aprotic/aprotic	49	–	
	0.3 M Et ₄ NBr ₄ /DMF	See catholyte	Al ₂ (C ₂ O ₄) ₃	2.5 V versus Ag/Ag ⁺	Undivided, aprotic	78	–	
	0.3 M Bu ₄ NBr/Ac	See catholyte	Al ₂ (C ₂ O ₄) ₃	2.5 V versus Ag/Ag ⁺	Undivided, aprotic	46	–	
Hg	DMF/H ₂ O	–	H ₂ C ₂ O ₄	–	Undefined	–	–	[74]
Pb	DMF/H ₂ O	–	H ₂ C ₂ O ₄ and C ₂ H ₄ O ₃	–	Undefined	–	–	
Fe plate	0.1 M Bu ₄ NClO ₄ /PC	See catholyte	H ₂ C ₂ O ₄ and CO	2.8 V versus Ag/AgCl	Two compartments, aprotic/aprotic	46 (H ₂ C ₂ O ₄) 15 (CO)	–	[89]
Cr plate	0.1 M Bu ₄ NClO ₄ /PC	See catholyte	H ₂ C ₂ O ₄ and CO	2.8 V versus Ag/AgCl	Two compartments, aprotic/aprotic	31 (H ₂ C ₂ O ₄) 11 (CO)	–	
Nb plate	0.1 M Bu ₄ NClO ₄ /PC	See catholyte	H ₂ C ₂ O ₄ and CO	2.8 V versus Ag/AgCl	Two compartments, aprotic/aprotic	7 (H ₂ C ₂ O ₄) 6 (CO)	–	
Mo plate	0.1 M Bu ₄ NClO ₄ /PC	See catholyte	H ₂ C ₂ O ₄ and CO	2.8 V versus Ag/AgCl	Two compartments, aprotic/aprotic	29 (H ₂ C ₂ O ₄) 14 (CO)	–	
Ti plate	0.1 M Bu ₄ NClO ₄ /PC	See catholyte	H ₂ C ₂ O ₄ and CO	2.8 V versus Ag/AgCl	Two compartments, aprotic/aprotic	19 (H ₂ C ₂ O ₄) 20 (CO)	–	
Ni plate	0.1 M Bu ₄ NClO ₄ /PC	See catholyte	CO	2.8 V versus Ag/AgCl	Two compartments, aprotic/aprotic	45	–	
Pd plate	0.1 M Bu ₄ NClO ₄ /PC	See catholyte	CO	2.8 V versus Ag/AgCl	Two compartments, aprotic/aprotic	51	–	
Pt plate	0.1 M Bu ₄ NClO ₄ /PC	See catholyte	CO	2.8 V versus Ag/AgCl	Two compartments, aprotic/aprotic	66	–	[89]
Cu plate	0.1 M Bu ₄ NClO ₄ /PC	See catholyte	CO	2.8 V versus Ag/AgCl	Two compartments, aprotic/aprotic	74	–	
Ag plate	0.1 M Bu ₄ NClO ₄ /PC	See catholyte	CO	2.8 V versus Ag/AgCl	Two compartments, aprotic/aprotic	77	–	
Au plate	0.1 M Bu ₄ NClO ₄ /PC	See catholyte	CO	2.8 V versus Ag/AgCl	Two compartments, aprotic/aprotic	83	–	
Cd plate	0.1 M Bu ₄ NClO ₄ /PC	See catholyte	CO	2.8 V versus Ag/AgCl	Two compartments, aprotic/aprotic	63	–	
Sn plate	0.1 M Bu ₄ NClO ₄ /PC	See catholyte	CO	2.8 V versus Ag/AgCl	Two compartments, aprotic/aprotic	81	–	
Pb plate	0.1 M Bu ₄ NClO ₄ /PC	See catholyte	H ₂ C ₂ O ₄	2.8 V versus Ag/AgCl	Two compartments, aprotic/aprotic	76	–	
Tl plate	0.1 M Bu ₄ NClO ₄ /PC	See catholyte	H ₂ C ₂ O ₄	2.8 V versus Ag/AgCl	Two compartments, aprotic/aprotic	70	–	
Hg plate	0.1 M Bu ₄ NClO ₄ /PC	See catholyte	H ₂ C ₂ O ₄	2.8 V versus Ag/AgCl	Two compartments, aprotic/aprotic	60	–	
In plate	0.1 M Bu ₄ NClO ₄ /PC	See catholyte	H ₂ C ₂ O ₄ (small production)	2.8 V versus Ag/AgCl	Two compartments, aprotic/aprotic	0.19	–	
Zn plate	0.1 M Bu ₄ NClO ₄ /PC	See catholyte	H ₂ C ₂ O ₄ (small production)	2.8 V versus Ag/AgCl	Two compartments, aprotic/aprotic	0.38	–	
Pt	0.1 M Bu ₄ NBF ₄ /AN	See catholyte	C ₂ O ₄ ²⁻	1.8–2.0 V versus Ag/Ag ⁺	Undivided, aprotic	–	–	[91]
Pb	0.1 M Bu ₄ NClO ₄ /DMF	See catholyte	Zn ₂ C ₂ O ₄	5–10 mA cm ²	Undivided, aprotic	80	–	[124]
Cu	Bu ₄ NBF ₄ /MeOH	See catholyte	CO and HCOOH	1.0–2.5 V	Undivided, protic	23 at 1 atm	–	[76]
Hg	0.2 M Bu ₄ NClO ₄ /DMF	See catholyte	C ₂ O ₄ ²⁻ and CO	1.6 mA cm ²	Two compartments	67 at 25 °C	–	[71]

Table 1. Continued.

Electrode	Catholyte ^{a)}	Anolyte	Major products	Cathode potential or j applied	Type of cell	FE [%]	Stability [min.]	References
Pb sheet	0.1 M Et ₄ NBr ₄ /MeOH	See catholyte	C ₂ HO ₃ ⁻ and C ₂ H ₃ O ₃ ⁻	1.7 V versus Ag/Ag ⁺	Undivided, protic	49 (C ₂ HO ₃ ⁻) 18 (C ₂ H ₃ O ₃ ⁻)	120	[72]
	0.1 M Et ₄ NBr ₄ /MeOH	See catholyte	C ₂ HO ₃ ⁻ and C ₂ H ₃ O ₃ ⁻	1.9 V versus Ag/Ag ⁺	Undivided, protic	50 (C ₂ HO ₃ ⁻) 34 (C ₂ H ₃ O ₃ ⁻)	120	
	0.1 M Et ₄ NBr ₄ /MeOH	See catholyte	C ₂ HO ₃ ⁻ and C ₂ H ₃ O ₃ ⁻	2.0 V versus Ag/Ag ⁺	Undivided, protic	52 (C ₂ HO ₃ ⁻) 46 (C ₂ H ₃ O ₃ ⁻)	120	
	0.1 M Et ₄ NBr ₄ /MeOH	See catholyte	C ₂ H ₃ O ₃ ⁻	2.3 V versus Ag/Ag ⁺	Undivided, protic	82	120	
Au foil	0.1 KOH/MeOH	See catholyte	CO and HCOOH	1.6–2.4 V versus SCE at –15 °C	Two compartments, protic/protic	1.6 V: 22 (CO) 14 (HCOOH) 1.8 V: 31 (CO) 11 (HCOOH) 2.0 V: 40 (CO) 11 (HCOOH) 2.2 V: 43 (CO) 9 (HCOOH) 2.4 V: 30 (CO) 14 (HCOOH)	–	[117]
Ti	0.1 M benzalkonium chloride/MeOH	1 M KHCO ₃ /H ₂ O	H ₂ , CH ₄ and CO	1.8 V versus SCE	Two compartments, protic/protic	114 (H ₂) 2 (CH ₄) 0.2 (CO)	–	[118]
Co	0.1 M benzalkonium chloride/MeOH	1 M KHCO ₃ /H ₂ O	H ₂ , CH ₄ and CO	1.5 V versus SCE	Two compartments, protic/protic	84 (H ₂) 2.3 (CH ₄) 0.2 (CO)	–	
Pt	0.1 M benzalkonium chloride/MeOH	1 M KHCO ₃ /H ₂ O	H ₂ and CH ₄	1.8 V versus SCE	Two compartments, protic/protic	94 (H ₂) 0.2 (CH ₄)	–	
Ag	0.1 M benzalkonium chloride/MeOH	1 M KHCO ₃ /H ₂ O	H ₂ , CH ₄ and CO	1.5 V versus SCE	Two compartments, protic/protic	41 (H ₂) 0.8 (CH ₄) 71 (CO)	–	
Au	0.1 M benzalkonium chloride/MeOH	1 M KHCO ₃ /H ₂ O	H ₂ , CH ₄ and CO	1.2 V versus SCE	Two compartments, protic/protic	10 (H ₂) 1.2 (CH ₄) 63 (CO)	–	
Zn	0.1 M benzalkonium chloride/MeOH	1 M KHCO ₃ /H ₂ O	H ₂ , CH ₄ and CO	1.6 V versus SCE	Two compartments, protic/protic	21 (H ₂) 0.6 (CH ₄) 64 (CO)	–	[118]
Sn	0.1 M benzalkonium chloride/MeOH	1 M KHCO ₃ /H ₂ O	H ₂ , CH ₄ and CO	1.5 V versus SCE	Two compartments, protic/protic	4.4 (H ₂) 1.8 (CH ₄) 28 (CO)	–	
Fe	0.1 M benzalkonium chloride/MeOH	1 M KHCO ₃ /H ₂ O	H ₂ , CH ₄ , C ₂ H ₄ and CO	1.1 V versus SCE	Two compartments, protic/protic	86 (H ₂) 1.3 (CH ₄) 0.2 (CO) 0.2 (C ₂ H ₄)	–	
Ni	0.1 M benzalkonium chloride/MeOH	1 M KHCO ₃ /H ₂ O	H ₂ , CH ₄ , C ₂ H ₄ , C ₂ H ₆ and CO	1.9 V versus SCE	Two compartments, protic/protic	95 (H ₂) 2.7 (CH ₄) 0.3 (CO) 0.5 (C ₂ H ₄) 0.3 (C ₂ H ₆)	–	

Table 1. Continued.

Electrode	Catholyte ^{a)}	Anolyte	Major products	Cathode potential or j applied	Type of cell	FE [%]	Stability [min.]	References
Cu	0.1 M benzalkonium chloride/MeOH	1 M KHCO ₃ /H ₂ O	H ₂ , CH ₄ , C ₂ H ₄ and CO	1.9 V versus SCE	Two compartments, protic/protic	54 (H ₂) 1.4 (CH ₄) 16 (CO) 3.5 (C ₂ H ₄)	–	
Pt (100)	Bu ₄ NClO ₄ /AN	See catholyte	C ₂ O ₄ ²⁻ and HCOO ⁻	3.1 V versus Ag/Ag ⁺	Three compartments	73 (C ₂ O ₄ ²⁻) 19 (HCOO ⁻)	–	[93]
Pt (111)	Bu ₄ NClO ₄ /AN	See catholyte	C ₂ O ₄ ²⁻ and HCOO ⁻	3.1 V versus Ag/Ag ⁺	Three compartments	57 (C ₂ O ₄ ²⁻) 8.8 (HCOO ⁻)	–	
Pt (110)	Bu ₄ NClO ₄ /AN	See catholyte	C ₂ O ₄ ²⁻ and HCOO ⁻	3.1 V versus Ag/Ag ⁺	Three compartments	74 (C ₂ O ₄ ²⁻) 13 (HCOO ⁻)	–	
Pt plate	0.1 M Bu ₄ NClO ₄ /AN	See catholyte	H ₂ C ₂ O ₄ and HCOOH	5 mA cm ²	Undivided	71.1 (H ₂ C ₂ O ₄) 11.2 (HCOOH)	–	[92]
Pb plate	0.1 M Bu ₄ NClO ₄ /AN	See catholyte	H ₂ C ₂ O ₄ , HCOOH, and CO	5 mA cm ²	Undivided	72.9 (H ₂ C ₂ O ₄) 19.6 (HCOOH) 8 (CO)	–	
Au plate	0.1 M Bu ₄ NClO ₄ /AN	See catholyte	HCOOH and CO	2.28 V versus Ag/Ag ⁺	Undivided	23.3 (HCOOH) 80.2 (CO)	–	
Pb	0.2 M Bu ₄ NClO ₄ /PC	See catholyte	C ₂ O ₄ ²⁻	2.5 V versus Ag/AgCl	Undivided, aprotic	–	–	[125]
Pb	0.1 M Bu ₄ NClO ₄ /AN	See catholyte	Zn ₂ C ₂ O ₄	2.2, 2.4, 2.6, and 2.8 V versus Ag	Undivided, aprotic	2.2 V: 64 2.4 V: 81 2.6 V: 92 2.8 V: 84	–	[39]
Pb sheet	0.1 M Bu ₄ NClO ₄ /AN	See catholyte	C ₂ O ₄ ²⁻	2.40 V versus Ag/Ag ⁺	Two compartments, aprotic/aprotic	73	180	[126]
	0.1 M [emim][Tf ₂ N] /AN	See catholyte	CO	2.25 V versus Ag/Ag ⁺	Two compartments, aprotic/aprotic	45	180	
Cu disk	0.1 M Bu ₄ NBF ₄ /AN	See catholyte	CO and CO ₃ ²⁻	2.4 V versus Ag/Ag ⁺	Undivided, aprotic	–	–	[73]
	0.1 M Bu ₄ NOTf/AN	See catholyte	CO and CO ₃ ²⁻	2.4 V versus Ag/Ag ⁺	Undivided, aprotic	–	–	
	0.1 M NaOTf /AN	See catholyte	CO and CO ₃ ²⁻	2.4 V versus Ag/Ag ⁺	Undivided, aprotic	–	–	
Au foil	0.1 M Bu ₄ NClO ₄ /PC	0.1 M H ₂ SO ₄	CO	2.5 V versus RHE	Two compartments, aprotic/protic	90	240	[127]
Pb sheet	0.9 M [TEA][4-MF-PhO]/AN	0.1 M H ₂ SO ₄	H ₂ C ₂ O ₄	2.6 V versus Ag/Ag ⁺	Two compartments, aprotic/protic	86	116	[120]
	0.1 M Bu ₄ NBF ₄ /AN	0.1 M H ₂ SO ₄	HCOOH and H ₂ C ₂ O ₄	2.6 V versus Ag/Ag ⁺	Two compartments, aprotic/protic	67 (HCOOH) 20 (H ₂ C ₂ O ₄)	–	
Pb sheet	0.1 M Bu ₄ NPF ₆ /AN	0.1 M H ₂ SO ₄	CO, HCOOH, and H ₂ C ₂ O ₄	2.6 V versus Ag/Ag ⁺	Two compartments, aprotic/protic	21 (CO) 66 (HCOOH) 11 (H ₂ C ₂ O ₄)	–	[120]
	0.1 M [BMIM][BF ₄]/AN	0.1 M H ₂ SO ₄	CO and HCOOH	2.6 V versus Ag/Ag ⁺	Two compartments, aprotic/protic	17 (CO) 80 (HCOOH)	–	
Pb rod	0.1 M Bu ₄ NBF ₄ /AN	See catholyte	Zn ₂ C ₂ O ₄ and CO	4 mA cm ²	Undivided, aprotic	80 (Zn ₂ C ₂ O ₄) 12 (CO)	30	[9]
Pb plate	0.25 M Bu ₄ NBF ₄ /AN	See catholyte	Zn ₂ C ₂ O ₄ and CO	10–40 mA cm ²	Flow cell	10 mA cm ² : 55 (Zn ₂ C ₂ O ₄) 20 mA cm ² : 40 (Zn ₂ C ₂ O ₄) 30 mA cm ² : 50 (Zn ₂ C ₂ O ₄)	30	

Table 1. Continued.

Electrode	Catholyte ^{a)}	Anolyte	Major products	Cathode potential or j applied	Type of cell	FE [%]	Stability References [min.]
Pb powder	0.25 M Bu ₄ NBF ₄ /AN (CO ₂ supplied at the back of the GDE)	See catholyte	C ₂ O ₄ ²⁻ and CO	20–80 mA cm ²	GDE flow cell	40 mA cm ² : 45 (Zn ₂ C ₂ O ₄)	30
						20 mA cm ² : 19 (C ₂ O ₄ ²⁻)	
						40 mA cm ² : 44 (C ₂ O ₄ ²⁻)	
						60 mA cm ² : 50 (C ₂ O ₄ ²⁻)	
Cu disk	0.5 M Bu ₄ NClO ₄ /DME	0.5 M H ₂ O + 0.5 M Bu ₄ NClO ₄ /DMF	CO and HCOOH	2.0–2.8 V versus Fc	Two compartments, aprotic/protic	80 mA cm ² : 53 (C ₂ O ₄ ²⁻)	– [95]
						2.0 V: 49 (HCOOH)	
						27 (CO)	
						2.2 V: 29 (HCOOH)	
						66 (CO)	
	0.5 M Bu ₄ NBF ₄ /DME	0.5 M H ₂ O + 0.5 M Bu ₄ NClO ₄ /DMF	CO and HCOOH	2.0–2.8 V versus Fc	Two compartments, aprotic/protic	2.4 V: 8 (HCOOH)	–
						90 (CO)	
						2.6 V: 96 (CO)	
						2.8 V: 6 (HCOOH)	
						92 (CO)	
Cu disk	0.5 M Bu ₄ NNO ₃ /DME	0.5 M H ₂ O + 0.5 M Bu ₄ NClO ₄ /DMF	CO and HCOOH	2.0–2.8 V versus Fc	Two compartments, aprotic/protic	2.0 V: 38 (HCOOH)	– [95]
						31 (CO)	
						2.2 V: 26 (HCOOH)	
						50 (CO)	
						2.4 V: 92 (CO)	
	0.5 M Bu ₄ NOTf/DME	0.5 M H ₂ O + 0.5 M Bu ₄ NClO ₄ /DMF	CO and HCOOH	2.0–2.8 V versus Fc	Two compartments, aprotic/protic	2.6 V: 98 (CO)	–
						2.8 V: 16 (HCOOH)	
						82 (CO)	
						2.0 V: 27 (HCOOH)	
						21 (CO)	
Cu disk	0.5 M Bu ₄ NTFSI/DME	0.5 M H ₂ O + 0.5 M Bu ₄ NClO ₄ /DMF	CO and HCOOH	2.0–2.8 V versus Fc	Two compartments, aprotic/protic	2.2 V: 10 (HCOOH)	– [95]
						43 (CO)	
						2.4 V: 3 (HCOOH)	
						82 (CO)	
						2.6 V: 92 (CO)	
	0.5 M Bu ₄ NTFSI/DME	0.5 M H ₂ O + 0.5 M Bu ₄ NClO ₄ /DMF	CO and HCOOH	2.0–2.8 V versus Fc	Two compartments, aprotic/protic	2.8 V: 19 (HCOOH)	– [95]
						77 (CO)	
						2.0 V: 16 (HCOOH)	
						33 (CO)	
						2.2 V: 99 (CO)	
Cu disk	0.5 M Bu ₄ NTFSI/DME	0.5 M H ₂ O + 0.5 M Bu ₄ NClO ₄ /DMF	CO and HCOOH	2.0–2.8 V versus Fc	Two compartments, aprotic/protic	2.4 V: 99 (CO)	– [95]
						2.6 V: 99 (CO)	
						2.8 V: 8 (HCOOH)	
						90 (CO)	
Cu disk	0.5 M Bu ₄ NTFSI/DME	0.5 M H ₂ O + 0.5 M Bu ₄ NClO ₄ /DMF	CO and HCOOH	2.0–2.8 V versus Fc	Two compartments, aprotic/protic	2.0 V: 22 (HCOOH)	– [95]
						42 (CO)	
Cu disk	0.5 M Bu ₄ NTFSI/DME	0.5 M H ₂ O + 0.5 M Bu ₄ NClO ₄ /DMF	CO and HCOOH	2.0–2.8 V versus Fc	Two compartments, aprotic/protic	2.2 V: 22 (HCOOH)	– [95]
						70 (CO)	

Table 1. Continued.

Electrode	Catholyte ^{a)}	Anolyte	Major products	Cathode potential or j applied	Type of cell	FE [%]	Stability References [min.]
						2.4 V: 94 (CO) 2.6 V: 95 (CO) 2.8 V: 7 (HCOOH) 90 (CO)	
Pb wire	0.7 M Et ₄ NCl/PC	0.5 M H ₂ SO ₄	H ₂ C ₂ O ₄ , C ₂ H ₄ O ₃ , and HCOOH	2.5 V versus Ag/AgCl	Two compartments, aprotic/protic	71 (H ₂ C ₂ O ₄) 3 (C ₂ H ₄ O ₃) 7 (HCOOH)	240 [42]
	0.1 M Et ₄ NCl/AN	0.5 M H ₂ SO ₄	H ₂ C ₂ O ₄ and HCOOH	2.5 V versus Ag/AgCl	Two compartments, aprotic/protic	6 (H ₂ C ₂ O ₄) 82 (HCOOH)	300
	0.1 M Et ₄ NCl/AN	0.1 M Et ₄ NCl/AN	H ₂ C ₂ O ₄	2.5 V versus Ag/AgCl	Two compartments, aprotic/protic	82	300
	0.1 M Bu ₄ NClO ₄ /PC	0.5 M H ₂ SO ₄	H ₂ C ₂ O ₄ and HCOOH	2.6 V versus Ag/AgCl	Two compartments, aprotic/protic	39 (H ₂ C ₂ O ₄) 38 (HCOOH)	270
Pb plate	0.7 M Et ₄ NCl/PC	0.5 M H ₂ SO ₄	H ₂ C ₂ O ₄ , C ₂ H ₂ O ₃ , C ₂ H ₄ O ₃ and HCOOH	2.3, 2.4 and 2.7 V versus Ag/AgCl	Flow cell	2.3 V: 75 (H ₂ C ₂ O ₄) 20 (HCOOH) 2.4 V: 55 (H ₂ C ₂ O ₄) 8 (C ₂ H ₂ O ₃) 7 (C ₂ H ₄ O ₃) 21 (HCOOH) 2.7 V: 43 (H ₂ C ₂ O ₄) 8 (C ₂ H ₄ O ₃) 32 (HCOOH)	300 [42]

^{a)}[emim][Tf₂N]: 1-ethyl-3-methylimidazolium bis(trifluoromethylsulfonyl)imide; [TEA][4-MF-PhO]: 4-(methoxycarbonyl) phenol tetraethylammonium; Ac: acetone; AN: acetonitrile; BMIM: 1-Butyl-3-methylimidazolium; Bu₄N: tetrabutylammonium; DCM: dichloromethane; DME: 1,2 dimethoxyethane; DMF: dimethylformamide; Et₄N: tetraethylammonium; MeOH: methanol; OTf: Triflate; PC: propylene carbonate; PC: propylene carbonate; TFSI: bistriflimide. –Information not reported.

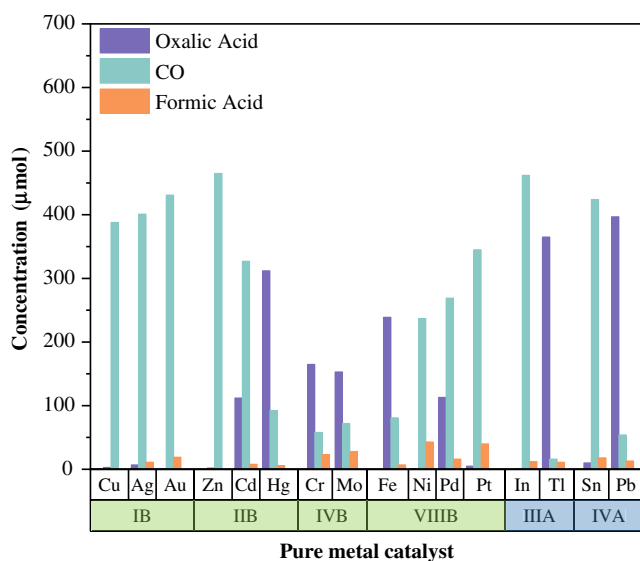


Figure 4. Products obtained from CO₂ reduction in propylene carbonate (PC) 0.1 M tetraethylammonium perchlorate (Bu₄NClO₄ClO₄) for various metal electrodes (organized by groups) at 2.8 V versus Ag/Ag^p. Transition metals are highlighted in green and post-transition metals are in blue. Adapted with permission.^[89] Copyright 1987, Chemical Society of Japan.

Figure 4 shows the comparison of the amount of product and selectivity for some metals evaluated by Ikeda et al.

Even though this classification is more complete and currently accepted,^[90] it is not consensual. Pt electrode,^[91–93] considered by Ikeda et al. as a selective catalyst to carbon monoxide, was efficient for eCO₂RR to oxalate. The first to show oxalic acid production using platinum electrodes was Desilvestro and Pons^[91] through an in situ FTIR spectroelectrochemistry study. After that, Hoshi et al.^[93] and Tomita et al.^[92] proved that Pt could produce oxalic and formic acid. Hoshi et al. study showed that the activity depends on the crystal orientation, and the following order of the activity for eCO₂RR is Pt (110) < Pt (111) < Pt (100). Considering the products, for oxalic acid, Pt (100) exhibited a partial current density twice as higher as Pt (110), and for formic acid, Pt (100) was three times higher than Pt (110). Tomita et al. demonstrated that Pt could reduce CO₂ to oxalic acid with similar faradaic efficiency to the Pb electrode. The Pb-like behavior of the Pt electrode on the eCO₂RR in an aprotic medium was attributed to the strong adsorption of CO on the platinum surface.^[94] According to them, the surface of the Pt electrode is covered with CO, reduced from CO₂, and the intermediate CO₂^{•-} is not adsorbed on the Pt surface, then two CO₂^{•-} (not adsorbed) coupled, leading to the formation of oxalic acid.

Besides pure Pt catalyst, other metals follow the same classification made by Ikeda et al., as shown in Table 1. Unlike an aqueous medium, copper does not exhibit outstanding performance in reducing CO₂ into C₂₊ products in an organic electrolyte.^[73,89,95] The main products reported for Cu are carbon monoxide and carbonate. In some cases, copper can reduce CO₂ to formic acid, as demonstrated by Gomes et al.^[95] The formic acid formation was assigned to the solvation effects of the supporting electrolyte on the stabilization of the intermediates, especially at lower reductive potentials, and not to an innate characteristic of the metal catalyst.

Among the catalyst that produces oxalic acid as the main product (Pb, Tl, and Hg), the Pb electrode stands out with higher product formation and faradaic efficiency (FE > 90%).^[89] As seen in Table 1, until today, Pb is the most studied catalyst to use in electrolytes with none or low proton viability to obtain multicarbon compounds from CO₂.^[7,9,39] Even shifting the selectivity by changing the electrochemical reaction conditions, like cell design, supporting electrolyte, solvent, potential or current density, oxalic acid is always expected. Higher faradaic efficiency (>50%) is found for Pb electrodes.^[9] That occurs because pure lead and mercury electrodes are chemically inert and have no significant interaction with the intermediate. Thus, CO₂ is adsorbed in the metal surface to form the intermediate that desorbs and dimerizes in the electrolyte,^[63] which is why controlling proton concentration is crucial to C₂₊ products.

Interestingly, Pb is the only pure metal that can reduce CO₂ to oxalic acid and oxalic acid to carboxylic acids in substantial amounts,^[72] leading to the formation of more complex C₂ molecules that can be used as a base to synthesize plenty of other organic compounds of industrial importance, such as the production of agrochemicals, cosmetic and pharmaceutical ingredients, and polymers.^[16] For Pb electrodes, time and potential is the factor predominant to the consecutive reduction of oxalic acid. Eggins et al.^[72] demonstrated that by changing the electrolysis potential and time, it was possible to switch the primary product from oxalate to glyoxylate and glycolate, all with good yields. At longer times of eCO₂RR, glyoxylate was formed

and consecutively reduced to glycolate, obtaining a mixture of glyoxylate and glycolate as leading products. The main product was only glycolate at a higher potential (−2.3 V vs Ag/Ag⁺).

Stainless steel alloys have also been studied, showing promising results for C₂₊ products. In the first publication of CO₂ reduction on an aprotic medium, Kaiser and Heitz^[41] proposed stainless steel as a cathode to obtain oxalic and carboxylic acids from CO₂ reduction since two other works can be found in the literature using stainless steel with different composition and cell design (see Table 2). Fischer et al.^[7] used high-alloy steel (18% Cr–8% Ni) as the cathode in a micro-pilot experiment to eCO₂RR for 100 h and obtained a faradaic efficiency of 90% to zinc oxalate (Zn₂C₂O₄) using a sacrificial anode (Zn plate). In a more recent publication, using the same strategy, Subramanian et al.^[40] used a stainless steel 304L cathode in ACN for the efficient production of oxalic acid. To higher yield of zinc oxalate (FE: 73%), the author suggested three essential factors, 1) minimizing the water content in the electrolyte solution; 2) operating at an optimum current density of 15 mA cm^{−2}; and 3) maintaining a pressure of 2 bar. Higher current density led to the solvent decomposition and formation of glycolate, reducing the oxalate yield.

Metal-based catalysts have also been studied for the electrochemical conversion of CO₂ to multicarbon compounds in a nonaqueous medium aiming to reduce or avoid using Pb as the cathode due to its toxicity and lower the overpotential for the eCO₂RR to C₂₊ products. Although the efficiencies still are not comparable to pure metal catalysts, the few publications (see Table 3) have some notable materials. A metal–organic framework (MOF) based on copper efficiently reduced CO₂ to oxalic acid.^[75] Kumar et al.^[75] achieved FE = 51% by using a MOF derived from benzene-1,3,5-tricarboxylic acid (BTC) combined with copper. Due to the MOF structure, the authors reduce the overpotential of eCO₂RR (−1.12 V versus Ag/Ag⁺) compared with the pure metal catalyst.^[95] Also, MOF structure played an essential role in stabilizing the adduct, favoring the dimerization of CO₂^{•−} formed from the 2-electron reduction of CO₂ in the

Table 2. Stainless steel catalysts, products, and cell configuration for eCO₂RR in nonaqueous electrolyte.

Electrode	Catholyte ^{a)}	Anolyte	Major products	Cathode potential or j applied	Type of cell	FE [%]	Stability [min.]	References
Cr–Ni–Mo alloy steel (18% Cr–10% Ni–2% Mo)	AN, PC (dry), PC (H ₂ O traces)	H ₂ SO ₄	HCOOH, H ₂ C ₂ O ₄ , C ₂ H ₂ O ₃ , and C ₂ H ₄ O ₃	5 mA cm ²	Three compartments	PC (dry): 61 (H ₂ C ₂ O ₄) PC (H ₂ O traces): 35 (H ₂ C ₂ O ₄)	–	[41]
High-Alloy Steel (18% Cr–8% Ni)	0.3 M Bu ₄ NClO ₄ /DMF	1 M NaCl/H ₂ O	H ₂ C ₂ O ₄	2.7 V versus Ag/Ag ⁺	Two compartments, aprotic/protic	32	–	[7]
	0.3 M Bu ₄ NClO ₄ /DMF	See catholyte	Zn ₂ C ₂ O ₄	2.5 V versus Ag/Ag ⁺	Undivided, aprotic	72	–	
	0.2 M Bu ₄ NBr ₄ /AN	See catholyte	Zn ₂ C ₂ O ₄	2.5 V versus Ag/Ag ⁺	Undivided, aprotic	87	–	
	0.2 M Et ₄ NBr ₄ /PC	See catholyte	Al ₂ (C ₂ O ₄) ₃	3–4 V versus Ag/Ag ⁺	Undivided, aprotic	68	–	
Stainless steel 304L	0.2 M Et ₄ NBr ₄ /DMF	See catholyte	Al ₂ (C ₂ O ₄) ₃	3–4 V versus Ag/Ag ⁺	Undivided, aprotic	81	–	
	0.2 M Bu ₄ NClO ₄ /AN	See catholyte	Zn ₂ C ₂ O ₄	5, 10, 15, and 30 mA cm ²	Undivided, aprotic	5 mA cm ² : 42	60	[40]
						10 mA cm ² : 46		
						15 mA cm ² : 51		
30 mA cm ² : 81								

^{a)}PC: propylene carbonate; DMF: dimethylformamide; AN: acetonitrile; Bu₄N: tetrabutylammonium; Et₄N: tetraethylammonium. –Information not reported.

Table 3. Metal-Based catalysts, synthesis method, and products for eCO₂RR in nonaqueous electrolyte.

Electrode	Catholyte ^{a)}	Catalyst synthesis	Major products	Cathode potential or j applied	Type of cell	References
Cu ₃ (BTC) ₂ (MOF film)	0.01 M Bu ₄ NBF ₄ /DMF	Electrosynthesis method	H ₂ C ₂ O ₄	2.5 V versus Ag/Ag ⁺	Undivided, aprotic	[75]
MoO ₂ /Pb	0.1 M Bu ₄ NPF ₆ /AN	Commercial	H ₂ C ₂ O ₄ , HCOOH, and CO	2.45 V versus Fe/Fc	Undivided, aprotic	[67]
TiO ₂	0.1 M Bu ₄ NClO ₄ /AN	Commercial	CO and C ₂ O ₄ ²⁻	1.8 V versus Ag/Ag ⁺	Undivided, aprotic	[114]
Pb _m Sn _n O _x /C	0.2 M Bu ₄ NClO ₄ /AN	One-pot method	C ₂ O ₄ ²⁻	1.7–2.5 V versus Ag/Ag ⁺	Undivided, aprotic	[63]
PbO/C	0.2 M Bu ₄ NClO ₄ /AN	Impregnation method with	C ₂ O ₄ ²⁻ and CO	1.7–2.5 V versus Ag/Ag ⁺	Undivided, aprotic	
SnO/C	0.2 M Bu ₄ NClO ₄ /AN	NaOH reflux	CO	1.7–2.5 V versus Ag/Ag ⁺	Undivided, aprotic	

^{a)}DMF: dimethylformamide; AN: acetonitrile; Bu₄N: tetrabutylammonium; BTC: benzene-1,3,5-tricarboxylic acid.

metal center, and Cu was capable of selectivity reducing CO₂ to oxalic acid.

Furthermore, combining different metals seems a promising strategy to develop catalysts with low Pb atoms to eCO₂RR in organic media. Using a commercial molybdenum oxide supported on a Pb pellet, Oh et al. (2014)^[67] reduced the overpotential from –2.5 to 2.0 V (vs Fe/Fc⁺). A higher current density was observed, and oxalic acid was produced with an FE of about 45% at –2.45 V. Another catalyst composed of Pb and Sn exhibited low overpotential and high selectivity in eCO₂RR to oxalate. Cheng et al.^[63] achieved the maximum oxalate Faradaic efficiency of 85.1% obtained at –1.9 V versus Ag/Ag⁺, comparable to bare Pb catalyst (FE > 90%).^[9] Different from bare Pb catalysts, a synergistic effect was observed for lead-tin oxides. The synergy for oxalate formation was confirmed by varying the Sn/Pb ratios. The authors suggested that this synergy occurs due to the Pb atoms in PbSn alloy being incorporated in the SnO_x lattice, which is easily reduced to Pb⁰. In this sense, Cheng et al. proposed a mechanism to explain the superior activity of lead-tin oxide. Initially, Pb ions in lead-tin oxides undergo reduction to form a Pb⁰-SnO_x composite structure; CO₂ is adsorbed on the Pb⁰ surface and forms CO₂^{•-} by the acceptance of one electron. The radical ion intermediate is then stabilized by SnO_x octahedral, leading to a couple with a neighboring CO₂^{•-} forming a C–C bond. The combination of Pb⁰ and oxidized Sn create a synergistic effect that favors a local configuration that stabilizes the CO₂ intermediates, lowering the overpotential for oxalate formation.

As can be seen, researchers have focused on studying and understanding the selectivity of pure metal catalysts to eCO₂RR in an organic medium. However, alternative electrocatalysts in the nonaqueous electrolyte are still poor.^[9] Despite the limited number of publications about alternative and efficient electrocatalysts for the electroreduction of CO₂ in organic media,^[7,40,41,63,67,75] they have provided new insights that can be used for the development of an efficient and sustainable catalyst to convert carbon dioxide into C₂₊ value-added products.

7. Strategies for Higher Selectivity Electrocatalysts for C₂₊ Products

Similarly to the aqueous medium, the activity and selectivity of the electrocatalyst can be majority determined by the cathode material,^[96,97] as shown in the previous section. Different

strategies have been used to modify the cathode selectivity, like morphology control,^[96–98] surface modification,^[99,100] defect engineering,^[101] electrolyte, ion effects,^[102] ionic liquids, and cell configuration. Other sessions have already discussed some of these strategies to change the selectivity of the eCO₂RR to C₂₊. Therefore, this topic focuses exclusively on catalyst modification strategies for nonaqueous media that have evidence to turn the selectivity of the reaction. Other rational-designed strategies, primarily used in the aqueous system, can be found in the survey published by Zhang and co-authors.^[103]

The redox potential for the intermediate formation in nonaqueous media is very high. Still, it can be significantly decreased if the CO₂^{•-} intermediate is stabilized by the adsorption on the catalyst surface. Some modifications on the catalyst have focused on improving the intermediate stability to favor the C–C coupling. Morphology control has been proven to be an efficient strategy for modulating the activity and selectivity of lead electrodes.^[104] Pander et al. demonstrated that a rough surface with contiguous, rounded features presented higher selectivity to formate in an aqueous medium due to the wafer morphology owing to more exposed edges. Although using Pb cathodes with controlled morphologies was not applied to nonaqueous media, König et al.^[9] suggested a similar behavior for an apparent increase in activity to oxalate formation in nonaqueous electrolytes. Thus, controlling morphology, like nanostructuring, increases activity either through a local chemical environment that stabilizes the intermediates and/or through a higher concentration of active sites that could favor the dimerization of the CO₂^{•-} intermediates to the oxalate formation.

Changing the composition of the catalyst has become an efficient strategy to achieve better catalytic performances. Although metal oxides presented problematic stability at a negative potential, the target design of their structure and morphology can turn the catalytic activity for CO₂ reduction and compensate for stability problems.^[105,106] Oh et al. demonstrated that molybdenum oxide is active in reducing CO₂ to oxalic acid. In contrast, the pure metallic molybdenum shows no significant catalytic current due to defects in the metal oxide that improve the adsorption of CO₂ on the catalyst surface.^[67,106] The combination of metal oxides is also an emerging strategy to enhance catalytic performance.^[106] Cheng et al.^[63] researched the catalytic activity of tin and lead oxide nanoparticles supported on carbon black. The combination of an active metal (Pb) for the formation of C₂ product (oxalic acid) with Sn oxide, active only to CO

production, exhibited higher catalytic performance than the pure lead oxide nanoparticle since the incorporation of CO formation metals can stabilize the CO_2^{*} intermediate by adsorption in nonaqueous electrolytes.^[90] A varied atomic ratio was investigated for lead/tin oxides, and the tin oxide composite demonstrated high catalytic activity with the proper balance. These composite catalysts showed synergy between multi-nuclear catalytic centers similar to metal complexes, decreasing the onset potentials for oxalate production.

A strategy to improve the reduction of CO_2 to more complex molecules in a nonaqueous medium was suggested by Garcia et al.^[78] According to their results Ag electrode is capable of catalyzing the dimerization of glyoxylate anion radical to tartaric acid. As demonstrated by some authors, glyoxylate anion can be obtained from the reduction of oxalic acid reduced from CO_2 . Therefore, incorporating Ag on a catalyst efficient to obtain oxalic acid from CO_2 could favor the production of tartaric acid from eCO_2RR and become a sustainable electrochemical route to tartaric acid. Besides the strategies reported, the hydrophobic microenvironment is also helpful for C_{2+} products, allowing sufficient time for the C–C coupling reaction. In this sense, rational catalyst design focusing on the proper coverage of the intermediates with a hydrophobic microenvironment could also be viable for future directions.^[107]

Besides morphology control, the other strategies cited have not been extensively studied, and further investigation is needed. The synergy of metals other than tin and Pb should be fully explored to understand the critical characteristic that favors the selectivity for C–C coupling. It is also important to emphasize that using Ag on the catalyst in eRRCO_2 in an organic electrolyte can work in two ways, as a catalyst for consecutive reduction of oxalate to more complex molecules or/and as a catalyst for CO_2 reduction to C_1 products (CO and CH_4) and deeply investigations are required. Additionally, surface modification on the catalyst to turn it more hydrophobic can stabilize the intermediate and favor its coupling, as demonstrated for homogeneous catalysts. In this sense, using hydrophobic single-atom or polymer-modified catalysts can improve the C_{2+} product formations even though nothing was found in the literature using an organic solvent as a catholyte.

In aqueous solutions, artificial intelligence (AI) and machine learning (ML) has been shown as efficient tools to accelerate and improve multimetallic electrocatalyst design for CO_2 reduction.^[108–110] This technology has already demonstrated its potential in multiple fields.^[109] It could be an interesting implement in developing electrocatalysts aiming to reduce the overpotential and stabilize the intermediate CO_2^{*} to favor the C–C coupling and obtain products like oxalic acid, glycolic acid, glyoxylic acid, and beyond. However, it is essential to cite that no references reporting the utilization of AI/ML for nonaqueous CO_2 reduction have been found, to the best of our knowledge.

8. Solvent Influence

The choice of supporting electrolytes is essential and highly complex. Factors such as pH, ionic nature, and concentration directly affect the kinetic and thermodynamic phenomena involved in the reaction, as they can alter the CO_2 solubility and speciation

in the reaction medium, as well as the electron and ion transport involved.^[111] The CO_2RR follows in a series of physical and chemical steps, which include 1) CO_2 adsorption and activation; 2) toward product desorption; and 3) at the active sites of the catalyst, i.e., the chemical environment where this occurs can alter the preferred pathway.

As mentioned earlier, the reaction mechanisms themselves change with the solvent.^[112] The reduction of CO_2 in protic solvent passes by the adsorption of CO_2 on the catalyst surface, followed by conversion to $^*\text{CO}$ and $^*\text{COH}$ rather than $^*\text{CHO}$. According to the authors, the $^*\text{CO}$ interacts with the transferred and activated protons on the catalyst's surface ($^*\text{H}$), forming the intermediate.^[113] This reaction step, called proton-coupled electron transfer (PCET), is listed as an essential step in the CO_2RR , as it makes it thermodynamically more favored with lower conversion potentials and interesting for processes involving multi-electron transfer (ethylene (12e^-), methane (8e^-), methanol (6e^-), etc.). However, reactions in protic solvents increase the competitive hydrogen evolution reaction (HER), which has an equilibrium electrode potential ($-0.42\text{ V vs SHE at pH} = 7$).

In contrast, eCO_2RR in a nonaqueous environment needs a large overpotential to activate the CO_2 to CO_2^{*} (-1.90 V vs SHE). The CO_2 molecule can adsorb on the surface of the electrocatalyst by two primary modes, $^*\text{COO}$ and $^*\text{OCO}$, depending on the affinity of the catalyst surface. Researchers generally agreed that metal (Pb, Bi, and Sn) prefers to bind CO_2 via carbon (i.e., $^*\text{COO}$) and generate CO or $^*\text{CO}$ intermediate, while oxides (TiO_2 , SnO_2 , and ZnO) bind CO_2 via oxygen (i.e., $^*\text{OCO}$).^[114] This different coordination mode is mainly because most oxides' stoichiometric ratio (Metal/Oxygen) is not reached, generating oxygen vacancies and metal cations on the catalyst surface.

Although few studied, the reaction under aprotic conditions has several advantages besides the high solubility of CO_2 and the absence of hydrogen evolution, among them the possibility of working over a wide potential range without parallel reactions occurring (Figure 5).

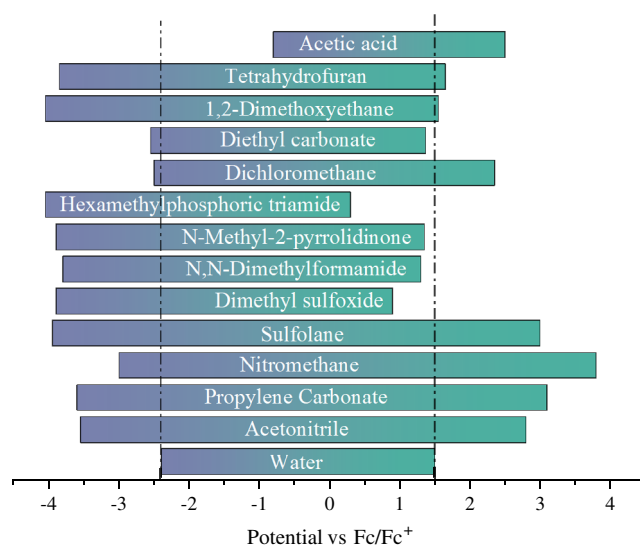


Figure 5. Potential windows in various solvents versus Fc/Fc^{b} . Obtained by voltammetry for a Pt electrode. Adapted with permission.^[112] Copyright 2009, John Wiley & Sons.

In addition to the solvent window, the variation in the standard potential of redox reactions is directly related to the variation in the solvation energy.^[112] Also, different cations and solvents can impact the $\text{CO}_2^{\cdot-}$ stability.^[115] Understanding cation/solvent interactions can enable the selective stabilization of the intermediate. Cencer and co-workers^[115] hypothesize that electrostatic and covalent/noncovalent interactions aligned with solvent stabilization and cation binding directly influence the inner-sphere solvation effects. They showed by ab initio molecular dynamics simulations that different cations and solvents affect the stability of the radical anion intermediate, and the eCO_2RR activity is correlated to the bulk solvation properties in DME and DMSO.

The use of methanol for CO_2 capture is already well known.^[116] Its use as an electrolyte in CO_2 reduction reactions was reported almost simultaneously by Eggins et al.^[72] and Kaneco et al.^[117] While Eggins and co-workers focused on the study of product selectivity, Kaneco et al. focused on the electrolyte influence. They evaluated the temperature dependence of CO_2 electrolysis using methanol and KOH as electrolytes. The reduction of CO_2 using gold as the working electrode reveals that the basicity of the medium and the low temperature suppress proton availability and shift the onset potential relative to experiments conducted in nitrogen, indicating the conversion of CO_2 to CO, HCOOH, reaching faradaic efficiency of up to 66.5% at -25°C at -2.4 V vs SCE , with CO_2/H_2 ratio of 4.1. On this same path, Ohta et al.^[118] and Oh et al.^[67] describe studies of the electroreduction of CO_2 in methanol with NaOH and at low temperatures, respectively. In both cases, the electrochemical study range involved high reduction potentials and high conversion rates demonstrating that electrochemical reactions conducted in methanol can lead to the formation of CH_4 , $\text{C}_2\text{O}_4^{2-}$, and HCOOH depending on the chemical environment.

In contrast, propylene carbonate is an attractive alternative organic solvent to obtain oxalate by the Sn electrode doped with Pb. In this case, the authors describe that a low charge of lead can bring a beneficial effect by the synergy of (Sn and Pb), allowing at -1.9 V vs Ag/Ag^+ , the dimerization of CO_2 molecules on the surface of the prepared catalyst (PbSnO_3/C) and faradaic efficiency of up to 85 at -1.9 V vs Ag/Ag^+ . However, the current density achieved is still low compared to experiments conducted in acetonitrile.^[63]

Solvent dependence in eCO_2RR was assessed by Berto et al.^[66] Their report showed that for a series of solvents (AN, THF, DMF, and PC), acetonitrile presented as an optimal solvent choice, giving the highest current at a smaller potential. A significant shift in the onset potential was not observed, but acetonitrile showed a current density 6 times greater than DMF. The current density was observed in the following order: $\text{AN} > \text{THF} > \text{PC} > \text{DMF}$. Even though acetonitrile demonstrated a better choice, the selectivity of each solvent for the electrochemical CO_2 reduction was not investigated. Also, the use of R_4N^+ cations appears to favor CO_2 reduction due to the hydrophobic environment at the cathodic chamber, and Li^+ salts, however, inhibit the CO_2RR by forming a film on the cathode surface.

The most commonly used organic electrolyte for CO_2 conversion is acetonitrile due to its stability, higher CO_2 solubility, and wide -2.7 to $+3\text{ V vs SCE}$ for Pt electrode in $0.1\text{ M TBAPF}_6/\text{MeCN}$ ^[119] König et al.^[9] describe that at -2.5 V vs Ag/Ag^+ , it is possible to achieve current density up to 80 mA cm^{-2} with

faradaic efficiency for oxalate production of 53% using a lead electrode. However, because it is a highly water-miscible solvent, it is recommended to dry the solvent with a molecular sieve or, in some cases, even distillation. This additional step can ensure clarity in interpreting the results since small amounts of water can change how CO_2 coordinates with the surface, the reaction overpotential, the mechanism, and the products. Although there is nothing set about the best solvent/electrolyte combination for eCO_2RR in a nonaqueous medium, some articles have studied a series of solvents and electrolytes mainly aiming to achieve higher current density,^[65,66,120] and the selectivity switching is usually not investigated.

9. Industrial Applications

The application of nonaqueous electrolytes at the industrial scale needs to be better described in the literature, mainly, patents can be found, and no techno-economic analysis is described. Therefore, this topic presented the process and industrial assemblies proposed by authors, some of which have never been evaluated in a pilot stage. In an industrial setup, a flow cell is usually used for direct CO_2 electrochemical reduction due to the facility attached to a continuous closed-loop industrial system^[121] and minimizing mass transport limitation,^[121,122] although flow electrolyzers are still not mature in the industry.^[121]

The first to propose an industrial process was Fischer and co-authors in 1981.^[7] They suggested using a Zn sacrificial anode in a flow cell setup with 4 purification steps. Following the formation of zinc oxalate, the product is separated in a filter and dissolved in a sulfuric acid solution. The purification of oxalic acid is done by liquid–liquid extraction with an organic solvent, and evaporation was used to obtain dry oxalic acid. The aqueous phase, containing zinc sulfate, is transferred to an electrolyzer to reduce the zinc ions for reuse. It is important to emphasize that no unwanted product was identified.

Another industrial process was developed and patented by Liquid Light Incpatent,^[85] now part of the Avantium company. They described a process with the electrochemical conversion of CO_2 in an aprotic media to oxalate its acidification to oxalic acid, purification using liquid–liquid extraction, and further reduction. A range of cell configurations and systems are reported, all of them with continuous flow. The acidification of oxalate salts is described in one or more steps. Interestingly, for the one-step process of converting $\text{CO}_2 \rightarrow \text{oxalate salts} \rightarrow \text{oxalic acid}$, the authors proposed the utilization of an anion exchange membrane capable of permeating the oxalate anion to the anodic chamber. In the anodic chamber, the GDE anode was fed with H_2 generating H^+ in the aprotic anolyte used to convert oxalate anion to oxalic acid. In an aqueous anolyte, the H^+ ions were formed by the oxygen evolution reaction. Considering that the use of an organic solvent and appropriate support electrolyte led to an increase in the cost of the industrial process, they also proposed a recovery method using electrochemical cells.

To industrially implement a large-scale process, not only techno-economic analysis plays an important role but also the optimization of carbon capture, utilization, and storage (CCUS) devices. In this aspect, artificial intelligence could be

used to provide optimal integration conditions of the different characteristics of industrial plants and the CCUS devices,^[123] such as heat, electricity, and load conditions.

10. Challenges for Future Research

The application of nonaqueous electrolytes in the eCO₂RR offers the potential of aiming alternative reaction products by controlling the H₂ evolution and increasing the CO₂ concentration in the reaction medium. However, the main challenges are with regard to the high cost of the reported nonaqueous media, their stability, and the typical fossil origin (e.g., acetonitrile, tetrahydrofuran, propylene carbonate, etc.). These aspects limit the utilization of these media, and though the results are promising, we still see more emphasis on aqueous electrolytes. The investigation also needs to define consensual catalysts, i.e., the investigation of materials that can address the large overpotential, slow electron transfer, unsatisfactory selectivity, and deactivation of electrodes in less than 100 h, factors that restrict practical use and technological commercialization. The development of new multicatalytic hybrid materials is also needed for use as a cathode to reduce CO₂.

Regarding reactor designs, they are generally based on the well-established systems used in aqueous electrolysis. However, the development of adequate ion separation membranes is still an issue that needs to be addressed. The authors describe utilizing a range of membranes, where Nafion stands out as the most reported. It is a problem since Nafion requires prehydration, i.e., water contamination is hardly avoided.

Furthermore, the use of low water concentration in the nonaqueous electrolyte has been shown to increase the activity of eCO₂RR without stimulating the competitive reaction of HER.^[36] The role of water concentration has yet to be fully understood regarding selectivity for C₂₊ products. Additionally, a demand for future research is to elucidate the differences in activity and selectivity to relate them to single parameters such as the CO₂ solubility or basicity of the solvent.

Acknowledgements

The author gratefully acknowledges the support of the RCGI—Research Centre for Greenhouse Gas Innovation, hosted by the University of São Paulo (USP) and sponsored by FAPESP—São Paulo Research Foundation (2014/50279-4, and 2020/15230-5) and Shell Brasil, and the strategic importance of the support given by ANP (the Brazilian National Oil, Natural Gas, and Biofuels Agency) under the R&D levy regulation. We also acknowledge the financial support of FAPESP (#2018/01258-5 and #2022/10255-5), the Coordenação de Aperfeiçoamento de Pessoal de Nível Superior—Brasil (CAPES)—Finance Code 001, and National Council for Scientific and Technological Development (CNPq).

Conflict of Interest

The authors declare no conflict of interest.

Keywords

CO₂ conversion, electroreduction, nonaqueous electrolytes, reaction mechanisms

Received: November 21, 2022

Revised: January 20, 2023

Published online:

- [1] M. Y. Lee, K. T. Park, W. Lee, H. Lim, Y. Kwon, S. Kang, *Crit. Rev. Environ. Sci. Technol.* **2020**, *50*, 769.
- [2] S. Fankhauser, S. M. Smith, M. Allen, K. Axelsson, T. Hale, C. Hepburn, J. M. Kendall, R. Khosla, J. Lezaun, E. Mitchell-Larson, M. Obersteiner, L. Rajamani, R. Rickaby, N. Seddon, T. Wetzler, *Nat. Clim. Change* **2021**, *12*, 15.
- [3] Overview of Greenhouse Gases | US EPA, <https://www.epa.gov/ghgemissions/overview-greenhouse-gases> (accessed: September 2022).
- [4] L. J. Müller, A. Kätelhön, S. Bringezu, S. McCoy, S. Suh, R. Edwards, V. Sick, S. Kaiser, R. Cuéllar-Franca, A. el Khamlichi, J. H. Lee, N. von der Assen, A. Bardow, *Energy Environ. Sci.* **2020**, *13*, 2979.
- [5] F. L. Souza, O. F. Lopes, E. V. Santos, C. Ribeiro, *Curr. Opin. Electrochem.* **2022**, *32*, 100890.
- [6] J. He, C. Janáky, *ACS Energy Lett.* **2020**, *5*, 1996.
- [7] J. Fischer, T. Lehmann, E. Heitz, *J. Appl. Electrochem.* **1981**, *11*, 743.
- [8] M. A. Murcia Valderrama, R. J. van Putten, G. J. M. Gruter, *Eur. Polym. J.* **2019**, *119*, 445.
- [9] M. König, S. H. Lin, J. Vaes, D. Pant, E. Klemm, *Faraday Discuss.* **2021**, *230*, 360.
- [10] J. Qiao, Y. Liu, F. Hong, J. Zhang, *Chem. Soc. Rev.* **2013**, *43*, 631.
- [11] W. Ye, X. Guo, T. Ma, *Chem. Eng. J.* **2021**, *414*, 128825.
- [12] R. Z. Zhang, B. Y. Wu, Q. Li, L. L. Lu, W. Shi, P. Cheng, *Coord. Chem. Rev.* **2020**, *422*, 213436.
- [13] M. Moura de Salles Pupo, R. Kortlever, *ChemPhysChem* **2019**, *20*, 2926.
- [14] F. Hussin, M. K. Aroua, *Rev. Chem. Eng.* **2021**, *37*, 863.
- [15] M. König, J. Vaes, E. Klemm, D. Pant, *iScience* **2019**, *19*, 135.
- [16] E. Schuler, M. Demetriou, N. R. Shiju, G. J. M. Gruter, *ChemSusChem* **2021**, *14*, 3636.
- [17] Y. Hori, *Mod. Aspects Electrochem.* **2008**, *42*, 89.
- [18] H. Yang, Q. Lin, C. Zhang, X. Yu, Z. Cheng, G. Li, Q. Hu, X. Ren, Q. Zhang, J. Liu, C. He, *Nat. Commun.* **2020**, *11*, 593.
- [19] H. Zbair, M. Baqais, A. Arab, M. Co, C. Alvarez-Galvan, H. Ait Ahsaine, M. Zbair, A. Baqais, M. Arab, *Catalysts* **2022**, *12*, 450.
- [20] F. Lucile, P. Cézac, F. Contamine, J. P. Serin, D. Houssin, P. Arpentinier, *J. Chem. Eng. Data* **2012**, *57*, 784.
- [21] A. Yasunishi, F. Yoshida, *J. Chem. Eng. Data* **1979**, *24*, 11.
- [22] L. Fan, C. Xia, F. Yang, J. Wang, H. Wang, Y. Lu, *Sci. Adv.* **2020**, *6*, eaay3111.
- [23] E. Boutin, M. Robert, *Trends Chem.* **2021**, *3*, 359.
- [24] M. Kan, Q. Wang, S. Hao, A. Guan, Y. Chen, Q. Zhang, Q. Han, G. Zheng, *J. Phys. Chem. C* **2022**, *126*, 1689.
- [25] C. Li, X. Tong, P. Yu, W. Du, J. Wu, H. Rao, Z. M. Wang, *J. Mater. Chem. A* **2019**, *7*, 16622.
- [26] W. Zhang, Y. Hu, L. Ma, G. Zhu, Y. Wang, X. Xue, R. Chen, S. Yang, Z. Jin, *Adv. Sci.* **2018**, *5*, 1700275.
- [27] T. Ahmad, S. Liu, M. Sajid, K. Li, M. Ali, L. Liu, W. Chen, *Nano Res. Energy* **2022**, *1*, e9120021.
- [28] L. Li, I. M. ul Hasan, J. Qiao, R. He, L. Peng, N. Xu, N. K. Niazi, J.-N. Zhang, F. Farwa, *Nano Res. Energy* **2022**, *1*, e9120015.
- [29] H. K. Lim, H. Kim, *Molecules* **2017**, *22*, 536.
- [30] J. Feng, S. Zeng, J. Feng, H. Dong, X. Zhang, *Chin. J. Chem.* **2018**, *36*, 961.

- [31] D. Faggion, W. D. G. Gonçalves, J. Dupont, *Front. Chem.* **2019**, 7, 102.
- [32] D. Yang, Q. Zhu, B. Han, *Innovation* **2020**, 1, 100016.
- [33] S. A. S. Mohammed, W. Z. N. Yahya, M. A. Bustam, M. G. Kibria, *Molecules* **2021**, 26, 6962.
- [34] T. E. Teeter, P. van Rysselberghe, *J. Chem. Phys.* **1954**, 22, 759.
- [35] B. E. Logan, E. Zikmund, W. Yang, R. Rossi, K. Y. Kim, P. E. Saikaly, F. Zhang, *Environ. Sci. Technol.* **2018**, 52, 8977.
- [36] A. V. Rudnev, U. E. Zhumaev, A. Kuzume, S. Vesztergom, J. Furrer, P. Broekmann, T. Wandlowski, *Electrochim. Acta* **2016**, 189, 38.
- [37] J. S. Jestilä, J. K. Denton, E. H. Perez, T. Khuu, E. Aprà, S. S. Xantheas, M. A. Johnson, E. Uggerud, *Phys. Chem. Chem. Phys.* **2020**, 22, 7460.
- [38] E. Liu, J. Li, L. Jiao, H. T. T. Doan, Z. Liu, Z. Zhao, Y. Huang, K. M. Abraham, S. Mukerjee, Q. Jia, *J. Am. Chem. Soc.* **2019**, 141, 3232.
- [39] W. Lv, R. Zhang, P. Gao, C. Gong, L. Lei, *J. Solid State Electrochem.* **2013**, 17, 2789.
- [40] S. Subramanian, K. R. Athira, M. A. Kulandainathan, S. S. Kumar, R. C. Barik, *J. CO₂ Util.* **2020**, 36, 105.
- [41] U. Kaiser, E. Heitz, *Ber. Bunsen Ges. Phys. Chem.* **1973**, 77, 818.
- [42] V. Boor, J. E. B. M. Frijns, E. Perez-Gallent, E. Giling, A. T. Laitinen, E. L. V. Goetheer, L. J. P. van den Broeke, R. Kortlever, W. de Jong, O. A. Moulto, T. J. H. Vlugt, M. Ramdin, *Ind. Eng. Chem. Res.* **2022**, 61, 14837.
- [43] A. Brunetti, E. Fontanovana, *J. Nanosci. Nanotechnol.* **2019**, 19, 3124.
- [44] T. Luo, S. Abdu, M. Wessling, *J. Membr. Sci.* **2018**, 555, 429.
- [45] B. Smitha, S. Sridhar, A. A. Khan, *J. Membr. Sci.* **2005**, 259, 10.
- [46] T. B. Ferriday, P. H. Middleton, *Int. J. Hydrogen Energy* **2021**, 46, 18489.
- [47] D. Henkensmeier, M. Najibah, C. Harms, J. Žitka, J. Hnát, K. Bouzek, *J. Electrochem. Energy Convers. Storage* **2021**, 18, 024001.
- [48] G. O. Larrazábal, P. Strøm-Hansen, J. P. Heli, K. Zeiter, K. T. Therkildsen, I. Chorkendorff, B. Seger, *ACS Appl. Mater. Interfaces* **2019**, 11, 41281.
- [49] R. Espiritu, B. T. Golding, K. Scott, M. Mamlouk, *J. Power Sources* **2018**, 375, 373.
- [50] K. Yang, X. Chu, X. Zhang, X. Li, J. Zheng, S. Li, N. Li, T. A. Sherazi, S. Zhang, *J. Membr. Sci.* **2020**, 603, 118025.
- [51] A. L. G. Biancolli, D. Herranz, L. Wang, G. Stehlíková, R. Bance-Soualhi, J. Ponce-González, P. Ocón, E. A. Ticianelli, D. K. Whelligan, J. R. Varcoe, E. I. Santiago, *J. Mater. Chem. A* **2018**, 6, 24330.
- [52] J. Walkowiak-Kulikowska, J. Wolska, H. Koroniak, *Phys. Sci. Rev.* **2017**, 2, <https://doi.org/10.1515/psr-2017-0018>.
- [53] B. Seger, K. Vinodgopal, P. V. Kamat, *Langmuir* **2007**, 23, 5471.
- [54] W. H. J. Hogarth, J. C. Diniz Da Costa, G. Q. Lu, *J. Power Sources* **2005**, 142, 223.
- [55] D. J. Kim, M. J. Jo, S. Y. Nam, *J. Ind. Eng. Chem.* **2015**, 21, 36.
- [56] P. Shirvanian, A. Loh, S. Sluijter, X. Li, *Electrochem. Commun.* **2021**, 132, 107140.
- [57] M. Wang, N. Preston, N. Xu, Y. Wei, Y. Liu, J. Qiao, *ACS Appl. Mater. Interfaces* **2019**, 11, 6881.
- [58] M. M. Alam, M. Hossain, Y. Mei, C. Jiang, Y. Wang, C. Y. Tang, T. Xu, *Desalination* **2021**, 497, 114779.
- [59] Q. Li, J. O. Jensen, R. F. Savinell, N. J. Bjerrum, *Prog. Polym. Sci.* **2009**, 34, 449.
- [60] J. A. Asensio, S. Borrós, P. Gómez-Romero, *Electrochem. Commun.* **2003**, 5, 967.
- [61] R. He, Q. Li, A. Bach, J. O. Jensen, N. J. Bjerrum, *J. Membr. Sci.* **2006**, 277, 38.
- [62] N. Gutiérrez-Guerra, J. L. Valverde, A. Romero, J. C. Serrano-Ruiz, A. de Lucas-Consuegra, *Electrochem. Commun.* **2017**, 81, 128.
- [63] Y. Cheng, P. Hou, H. Pan, H. Shi, P. Kang, *Appl. Catal., B* **2020**, 272, 118954.
- [64] M. Rudolph, S. Dautz, E. G. Jager, *J. Am. Chem. Soc.* **2000**, 122, 10821.
- [65] J. O. Bockris, J. C. Wass, *J. Electrochem. Soc.* **1989**, 136, 2521.
- [66] T. C. Berto, L. Zhang, R. J. Hamers, J. F. Berry, *ACS Catal.* **2015**, 5, 703.
- [67] Y. Oh, H. Vruble, S. Guidoux, X. Hu, *Chem. Commun.* **2014**, 50, 3878.
- [68] T. Kai, M. Zhou, Z. Duan, G. A. Henkelman, A. J. Bard, *J. Am. Chem. Soc.* **2017**, 139, 18552.
- [69] C. M. Hendy, G. C. Smith, Z. Xu, T. Lian, N. T. Jui, *J. Am. Chem. Soc.* **2021**, 143, 8987.
- [70] G. B. Stevens, T. Reda, B. Raguse, *J. Electroanal. Chem.* **2002**, 526, 125.
- [71] A. Gennaro, A. A. Isse, M. G. Severin, E. Vianello, I. Bhugun, J. M. Savéant, *J. Chem. Soc., Faraday Trans.* **1996**, 92, 3963.
- [72] B. R. Eggins, C. Ennis, R. McConnell, M. Spence, *J. Appl. Electrochem.* **1997**, 27, 706.
- [73] M. C. Figueiredo, I. Ledezma-Yanez, M. T. M. Koper, *ACS Catal.* **2016**, 6, 2382.
- [74] C. Amatore, J. M. Savéant, *J. Am. Chem. Soc.* **1981**, 103, 5021.
- [75] R. Senthil Kumar, S. Senthil Kumar, M. Anbu Kulandainathan, *Electrochem. Commun.* **2012**, 25, 70.
- [76] T. Saeki, K. Hashimoto, A. Fujishima, N. Kimura, K. Omata, *J. Phys. Chem.* **1995**, 99, 8440.
- [77] B. R. Eggins, C. Ennis, J. T. S. Irvine, *J. Appl. Electrochem.* **1994**, 24.
- [78] A. C. Garcia, C. Sánchez-Martínez, I. Bakker, E. Goetheer, *ACS Sustainable Chem. Eng.* **2020**, 8, 10454.
- [79] B. S. Ooi, *Encyclopedia of Membranes*, Springer, Heidelberg, Germany **2016**, pp. 1431–1432, https://doi.org/10.1007/978-3-662-44324-8_1782.
- [80] Y. S. Aşçı, U. Dramur, M. Bilgin, *J. Mol. Liq.* **2017**, 248, 391.
- [81] C. Mutschler, J. Aparicio, I. Mokbel, M. Capron, P. Fongarland, M. Araque, C. Nikitine, *Front. Chem.* **2022**, 10, 909380.
- [82] R. Ban, M. Liu, Y. Qin, H. Wang, D. Cui, *Trans. Tianjin Univ.* **2012**, 18, 320.
- [83] M. Matsumoto, T. Otono, K. Kondo, *Sep. Purif. Technol.* **2001**, 24, 337.
- [84] D. Datta, Y. S. Aşçı, A. F. Tuyun, *J. Chem. Eng. Data* **2015**, 60, 3262.
- [85] T. Zbigniew, C. E. Barton, K. J. J. T. Kyle, K. K. A. P. Rishi, B. Alexander, S. Narayanappa, L. George, K. T. J. M. Paul, Z. H. U. Yizu, Method and System for Production of Oxalic Acid and Oxalic Acid Reduction Products, US9267212B2 **2016**.
- [86] R. Francke, B. Schille, M. Roemelt, *Chem. Rev.* **2018**, 118, 4631.
- [87] F. Franco, C. Rettenmaier, H. S. Jeon, B. Roldan Cuenya, *Chem. Soc. Rev.* **2020**, 49, 6884.
- [88] N. W. Kinzel, C. Werlé, W. Leitner, *Angew. Chem., Int. Ed.* **2021**, 60, 11628.
- [89] S. Ikeda, T. Takagi, K. Ito, *Bull. Chem. Soc. Jpn.* **1987**, 60, 2517.
- [90] Y. Hori, *Handbook of Fuel Cells*, John Wiley & Sons, Hoboken, New Jersey **2010**, <https://doi.org/10.1002/9780470974001.F207055>.
- [91] J. Desilvestro, S. Pons, *J. Electroanal. Chem. Interfacial Electrochem.* **1989**, 267, 207.
- [92] Y. Tomita, S. Teruya, O. Koga, Y. Hori, *J. Electrochem. Soc.* **2000**, 147, 4164.
- [93] N. Hoshi, T. Murakami, Y. Tomita, Y. Hori, *Electrochemistry* **1999**, 67, 1144.
- [94] Y. Tomita, Y. Hori, *Stud. Surf. Sci. Catal.* **1998**, 114, 581.
- [95] R. J. Gomes, C. Birch, M. M. Cencer, C. Li, S. B. Son, I. D. Bloom, R. S. Assary, C. Amanchukwu, *J. Phys. Chem. C* **2022**, 2022, 13595.
- [96] W. Zhang, C. Xu, Y. Hu, S. Yang, L. Ma, L. Wang, P. Zhao, C. Wang, J. Ma, Z. Jin, *Nano Energy* **2020**, 73, 104796.
- [97] Q. Yang, X. Liu, W. Peng, Y. Zhao, Z. Liu, M. Peng, Y. R. Lu, T. S. Chan, X. Xu, Y. Tan, *J. Mater. Chem. A* **2021**, 9, 3044.

- [98] W. Zhang, Y. Xia, S. Chen, Y. Hu, S. Yang, Z. Tie, Z. Jin, *Nano Lett.* **2022**, *22*, 3340.
- [99] W. Zhang, M. Jiang, S. Yang, Y. Hu, B. Mu, Z. Tie, Z. Jin, *Nano Res. Energy* **2022**, *1*, e9120033.
- [100] S. Lin, C. S. Diercks, Y. B. Zhang, N. Kornienko, E. M. Nichols, Y. Zhao, A. R. Paris, D. Kim, P. Yang, O. M. Yaghi, C. J. Chang, *Science* **2015**, *349*, 1208.
- [101] W. Zhang, Y. Hu, L. Ma, G. Zhu, P. Zhao, X. Xue, R. Chen, S. Yang, J. Ma, J. Liu, Z. Jin, *Nano Energy* **2018**, *53*, 808.
- [102] J. Shen, R. Kortlever, R. Kas, Y. Y. Birdja, O. Diaz-Morales, Y. Kwon, I. Ledezma-Yanez, K. J. P. Schouten, G. Mul, M. T. M. Koper, *Nat. Commun.* **2015**, *6*, 8177.
- [103] W. Zhang, Z. Jin, Z. Chen, *Adv. Sci.* **2022**, *9*, 2105204.
- [104] J. E. Pander, J. W. J. Lum, B. S. Yeo, *J. Mater. Chem. A* **2019**, *7*, 4093.
- [105] Y. Sun, Q. Wang, Z. Geng, Z. Liu, R. Yang, *Chem. Eng. J.* **2021**, *415*, 129044.
- [106] S. S. A. Shah, M. Sufyan Javed, T. Najam, C. Molochas, N. A. Khan, M. A. Nazir, M. Xu, P. Tsiakaras, S. J. Bao, *Coord. Chem. Rev.* **2022**, *471*, 214716.
- [107] Y. Cheng, P. Hou, X. Wang, P. Kang, *Acc. Chem. Res.* **2022**, *55*, 231.
- [108] N. Zhang, B. Yang, K. Liu, H. Li, G. Chen, X. Qiu, W. Li, J. Hu, J. Fu, Y. Jiang, M. Liu, J. Ye, *Small Methods* **2021**, *5*, 2100987.
- [109] A. Chen, X. Zhang, L. Chen, S. Yao, Z. Zhou, *J. Phys. Chem. C* **2020**, *124*, 22471.
- [110] A. Mazheika, Y. G. Wang, R. Valero, F. Viñes, F. Illas, L. M. Ghiringhelli, S. V. Levchenko, M. Scheffler, *Nat. Commun.* **2022**, *13*, 419.
- [111] V. J. Ovalle, M. M. Waegle, *J. Phys. Chem. C* **2021**, *125*, 18567.
- [112] K. Izutsu, *Electrochemistry in Non-Aqueous Solutions*, Wiley-VCH, Weinheim, Germany **2009**, p. 440.
- [113] H. Xiao, T. Cheng, W. A. Goddard, R. Sundararaman, *J. Am. Chem. Soc.* **2016**, *138*, 483.
- [114] N. E. Mendieta-Reyes, W. Cheuquepán, A. Rodes, R. Gómez, *ACS Catal.* **2020**, *10*, 103.
- [115] M. M. Cencer, C. Li, G. Agarwal, R. J. Gomes Neto, C. V. Amanchukwu, R. S. Assary, *ACS Omega* **2022**, *7*, 18131.
- [116] S. Kaneco, K. Iiba, M. Yabuuchi, N. Nishio, H. Ohnishi, H. Katsumata, T. Suzuki, K. Ohta, *Ind. Eng. Chem. Res.* **2002**, *41*, 5165.
- [117] S. Kaneco, K. Iiba, K. Ohta, T. Mizuno, A. Saji, *J. Electroanal. Chem.* **1998**, *441*, 215.
- [118] K. Ohta, M. Kawamoto, T. Mizuno, D. A. Lowy, *J. Appl. Electrochem.* **1998**, *28*, 717.
- [119] N. Elgrishi, K. J. Rountree, B. D. McCarthy, E. S. Rountree, T. T. Eisenhart, J. L. Dempsey, *J. Chem. Educ.* **2018**, *95*, 197.
- [120] Y. Yang, H. Gao, J. Feng, S. Zeng, L. Liu, L. Liu, B. Ren, T. Li, S. Zhang, X. Zhang, *ChemSusChem* **2020**, *13*, 4900.
- [121] D. Ma, T. Jin, K. Xie, H. Huang, *J. Mater. Chem. A* **2021**, *9*, 20897.
- [122] G. Li, Y. Liu, Q. Zhang, Q. Hu, W. Guo, X. Cao, Y. Dou, L. Cheng, Y. Song, J. Su, L. Huang, R. Ye, *J. Mater. Chem. A* **2022**, *10*, 19254.
- [123] H. Xi, X. Wu, X. Chen, P. Sha, *Appl. Energy* **2021**, *295*, 117069.
- [124] M. Chandrasekaran, T. Raju, V. Krishnan, *Bull. Electrochem.* **1992**, *8*, 124.
- [125] B. Eneau-Innocent, D. Pasquier, F. Ropital, J. M. Léger, K. B. Kokoh, *Appl. Catal. B* **2010**, *98*, 65.
- [126] L. Sun, G. K. Ramesha, P. V. Kamat, J. F. Brennecke, *Langmuir* **2014**, *30*, 6302.
- [127] J. Shi, F. X. Shen, F. Shi, N. Song, Y. J. Jia, Y. Q. Hu, Q. Y. Li, J. X. Liu, T. Y. Chen, Y. N. Dai, *Electrochim. Acta* **2017**, *240*, 114.



Eduardo A. Reis is a Ph.D. student at the University of São Paulo, São Carlos Institute of Chemistry, under the supervision of Dr. Caue Ribeiro. He obtained his bachelor's in chemistry with technological attributions at the Federal University of Mato Grosso and earned his master's degree in inorganic chemistry at the Federal University of São Carlos. Currently, his research focuses on electrocatalyst/ electrode preparation, optimization of electrochemical reactions, and devices for CO₂ conversion and energy storage.



Gelson T.S.T. da Silva received his Doctorate in chemistry at the Federal University of São Carlos, Brazil in 2019. Currently, he is a research fellow in the Interdisciplinary Laboratory of Electrochemistry and Ceramics (LIEC) of the Federal University of São Carlos (UFSCar). His research focuses on developing functional materials for carbon capture and utilization from photoelectrochemical technologies.



Elisabete I. Santiago is a senior researcher at the Nuclear and Energy Research Institute (IPEN) in São Paulo - Brazil. Her background is in electrochemistry focusing on new energies, such as fuel cells, electrolysis, methane, and carbon dioxide electrochemical conversion into added-value compounds. Recently, she is dedicated to the development of new generation of anion-exchange membranes produced via radiation-induced grafting.



Caue Ribeiro holds a Ph.D. in physical chemistry from the, Sao Carlos Federal University–UFSCar, Brazil, 2005, and is a materials engineer, UFSCar, 1999. Since 2007, he has been a senior researcher at the Brazilian Agriculture Research Corporation (Embrapa, Brazil). He has received the Chinese Academy of Sciences (CAS) President’s International Fellowship Initiative (PIFI) as visiting researcher and the Alexander von Humboldt Fellowship for Experienced Scientists (Germany) hosted at Forschungszentrum Jülich (2018 to 2020). His research interests are the development of photocatalysts for water decontamination and energy conversion and materials for controlled release of fertilizers.